MASSACHUSETTS INSTITUTE OF TECHNOLOGY
LINCOLN LABORATORY

DESCRIPTION OF THE AVON-TO-WESTFORD EXPERIMENT

R. K. CRANE

Group 61

TECHNICAL REPORT 483

29 APRIL 1971

LEXINGTON MASSACHUSETTS

The work reported in this document was performed at Lincoln Laboratory, a center for research operated by Massachusetts Institute of Technology. This work was sponsored by the National Aeronautics and Space Administration under Contract NAS 5-21544.

ERRATA SHEET

for Technical Report 483

The author has detected the following errors in Technical Report 483 (R. K. Crane, "Description of the Avon-to-Westford Experiment," 29 April 1971). Kindly insert this sheet into your copy of that report.

Page 2, Eq. (1), change

$\hat{u}_1 \cdot \underset{\approx}{\beta}_s \cdot \hat{u}_2$ to read $|\hat{u}_1 \cdot \underset{\approx}{S} \cdot \hat{u}_2|^2$

Page 3, fourth line, change

$\underset{\approx}{\beta}_s$ = tensor scattering cross section per unit volume

to read

$\underset{\approx}{S}$ = scattering amplitude tensor

and in Eq. (2), change

$\hat{u}_1 \cdot \underset{\approx}{\beta}_s(x) \cdot \hat{u}_2\,dx$ to read $|\hat{u}_1 \cdot \underset{\approx}{S}(x) \cdot \hat{u}_2|^2\,dx$

Page 4, Eqs. (3) and (4), change

$\hat{u}_1 \cdot \underset{\approx}{\beta}_s \cdot \hat{u}_2$ to read $|\hat{u}_1 \cdot \underset{\approx}{S} \cdot \hat{u}_2|^2$

also in Eq. (3), in the expression for D, change

$\hat{u}_1 \cdot \underset{\approx}{\beta}_s(x) \cdot \hat{u}_2\,dx$ to read $|\hat{u}_1 \cdot \underset{\approx}{S}(x) \cdot \hat{u}_2|^2\,dx$

and

$\hat{u}_1 \cdot \underset{\approx}{\beta}_s(r_1) \cdot \hat{u}_2$ to read $|\hat{u}_1 \cdot \underset{\approx}{S}(r_1) \cdot \hat{u}_2|^2$

and in the paragraph immediately following, change $\underset{\approx}{\beta}_s$ to read $\underset{\approx}{S}$ each time it appears.

Page 5, first line following Eq. (5), change

$\hat{u}_1 \cdot \underset{\approx}{\beta}_s \cdot \hat{u}_1$ to read $|\hat{u}_1 \cdot \underset{\approx}{S} \cdot \hat{u}_2|^2$

and in lines 2 and 3 of the next paragraph, change

$\hat{u}_1 \cdot \underset{\approx}{\beta}_s \cdot \hat{u}_2 D$ to read $|\hat{u}_1 \cdot \underset{\approx}{S} \cdot \hat{u}_2|^2 D$

also change Eq. (7) to read

$$\beta_s = |\hat{u}_1 \cdot \underset{\approx}{S} \cdot \hat{u}_2|^2 = |\hat{u}_1 \cdot (\hat{a}_1 \cos\varphi \hat{a}_2 + \hat{b}_1 \hat{b}_2) \cdot \hat{u}_2|^2 \frac{\pi^5 Z |\kappa|^2}{\lambda^4}$$

and add after "where,"

β_s = scattering cross section per unit volume

(OVER)

Page 6, Eq. (8), change

$$\hat{u}_1 \cdot (\hat{a}_1 \cos^2 \varphi a_2 + \hat{b}_1 \hat{b}_2) \cdot \hat{u}_2 \quad \text{to read} \quad |\hat{u}_1 \cdot (\hat{a}_1 \cos\varphi \hat{a}_2 + \hat{b}_1 \hat{b}_2) \cdot \hat{u}_2|^2$$

change Eq. (10) to read

$$\beta_s = |\hat{u}_1 \cdot (\hat{a}_1 \cos\varphi \hat{a}_2 + \hat{b}_1 \hat{b}_2) \cdot \hat{u}_2|^2 \frac{0.378 C_n^2}{\lambda^{1/3} (\sin\frac{\varphi}{2})^{11/3}}$$

and in Eq. (11), change

$$\hat{u}_1 \cdot (\hat{a}_1 \cos^2 \varphi \hat{a}_2 + \hat{b}_1 \hat{b}_2) \quad \text{to read} \quad |\hat{u}_1 \cdot (\hat{a}_1 \cos\varphi \hat{a}_2 + \hat{b}_1 \hat{b}_2) \cdot \hat{u}_2|^2$$

Page 16, in col. 1 of Table II, change

$$\hat{u}_1 \cdot \underset{\approx}{\beta}_s \cdot \hat{u}_2 D \quad \text{to read} \quad |\hat{u}_1 \cdot \underset{\approx}{S} \cdot \hat{u}_2|^2 D$$

Page 17, third paragraph, change

$$\hat{u}_1 \cdot \underset{\approx}{\beta}_s \cdot \hat{u}_2 D \quad \text{to read} \quad |\hat{u}_1 \cdot \underset{\approx}{S} \cdot \hat{u}_2|^2 D$$

each time it appears

Page 30, fifth line, change

$$\hat{u}_1 \cdot (\hat{a}_1 \cos^2 \varphi_i \hat{a}_2 + \hat{b}_1 \hat{b}_2) \cdot \hat{u}_2 \quad \text{to read} \quad |\hat{u}_1 \cdot (\hat{a}_1 \cos\varphi_i \hat{a}_2 + \hat{b}_1 \hat{b}_2) \cdot \hat{u}_2|^2$$

5 November 1971

Publications Office
M.I.T. Lincoln Laboratory
P.O. Box 73
Lexington, Massachusetts 02173

ABSTRACT

This report describes a Lincoln Laboratory experiment referred to as the Avon-to-Westford experiment which consisted of a series of bistatic scatter and radar measurements of the scattering cross section per unit volume of rain and thin turbulent layers. Results of the experiment are presented as average and rms values of the ratio of the bistatic scatter cross section as calculated using the radar data to the cross section as measured with the bistatic scatter system. The goal of the experiment was to test the precision of the approximate description of scattering due to rain and thin turbulent layers used in interference predictions.

The experiment utilized a 143-km, 4.515-GHz scatter path from Avon, Connecticut, to the Westford Communications Terminal and the Millstone Hill 1.295-GHz radar in Westford, Massachusetts. Scatter measurements were made using scattering angles ranging from 2° to 180°. System sensitivities allowed measurements of rain with Z_e greater than −5 dBZ (equivalent rain rate of 0.02 mm/hr) and C_{ne}^2 greater than $10^{-16} m^{-2/3}$. The maximum error in the estimation of the ratio of calculated-to-measured cross section is 2.7 dB.

CONTENTS

DESCRIPTION OF THE AVON-TO-WESTFORD EXPERIMENT

I. INTRODUCTION

The success of frequency sharing by several communication services depends upon the precision with which the statistics of interference between these services may be predicted. Pessimistic predictions will restrict the development of new services, and optimistic predictions will result in interference between services. Under the sponsorship of the Radio Frequency Interference and Propagation Program (RIPP) of the National Aeronautics and Space Administration, the Avon-to-Westford experiment was conducted to test the precision of the approximate descriptions of two of the propagation mechanisms – rain scatter and thin turbulent layer scatter – that may cause interference at centimeter and millimeter wavelengths. The experiment consisted of a series of simultaneous radar (backscatter) and transhorizon scatter (bistatic) measurements of scattering by both rain and thin turbulent layers. Radar measurements were made using the Millstone Hill L-band radar. Bistatic scatter measurements were made at C-band using a van-mounted transmitter located in Avon, Connecticut, and the Westford Communications Terminal in Westford, Massachusetts. The approximate descriptions of the scattering processes for rain and thin turbulent layers were investigated by comparing the signal strength values as measured with the bistatic system with those calculated using as a basis the simultaneous radar measurements, the approximate descriptions of the scattering cross section per unit volume for both mechanisms, and the bistatic radar equation.

Interference predictions as currently made are for conditions of either rain or no rain. No further separation by mechanism is made. The prediction of interference due to rain is generally based upon the use of climatological data, Rayleigh scattering theory, available attenuation coefficients, and an assumed distribution of scatterers in space.[1] In a previous report,[2] a simplified rain interference computation technique was proposed and preliminary X-band measurements on the Avon-to-Westford path were presented that supported the use of the approximate calculation procedure. The experiment described in this report provides a more extensive investigation of the assumptions used in the calculation procedure and provides support for the values of some of the parameters used in its application. The experimental program was directed at investigating the bistatic nature of scattering by hydrometeors and was not designed to provide climatological data. However, climatological data are required for the development of an interference prediction procedure.

Interference prediction in the absence of rain is currently accomplished by extrapolations based upon empirical data.[3,4] The data used as the basis for the prediction technique were, however, obtained at frequencies below those of interest, obtained using troposcatter systems which conform to only one of the many geometrical configurations of interest to the interference problem, and represent a combination of several transhorizon propagation mechanisms which will not be present in the same proportion for most interference problems. The extrapolation to centimeter and millimeter wavelength interference problems is not based upon separation into the relevant mechanisms and the use of the known properties of these mechanisms. The experimental program described in this report included an investigation of scattering by one of the non-rain mechanisms, thin turbulent layers, for a variety of geometrical configurations. This part of the experimental study was conducted to provide data for comparison with the current prediction method.

Additional results of the Avon-to-Westford experiment will be presented in four additional reports: Summer Rain Showers, Widespread Autumn Rain, Thin Turbulent Layers, and Summary of Results. This report includes the approximations developed for the calculation of transmission loss for use in interference prediction, the description of the technique used for calculating the estimate of the transmission loss for the Avon-to-Westford path, descriptions of the radar and bistatic scatter systems, and an error analysis. The measurements and analysis will be presented in later reports.

II. APPROXIMATIONS USED IN TRANSMISSION LOSS CALCULATION DUE TO SCATTERING

The transhorizon propagation mechanisms of importance to interference phenomena at centimeter and millimeter wavelengths are ducting, rain scatter, thin turbulent layer scatter, and terrain diffraction. Two of the mechanisms (rain and thin layer scatter) refer to scattering from an extended region of space and are the subject of the Avon-to-Westford experimental program. Both hydrometeor and turbulent scatter may be described at centimeter wavelengths, by single scattering from a volume of scatterers. The bistatic radar equation then can be used to relate the transmission loss for a bistatic scattering system to the per-unit volume scattering properties of the rain or turbulent regions. The per-unit volume scattering properties may also be deduced from radar measurements. Simultaneous radar and bistatic scattering measurements of the same scattering volume will provide information on the scattering angle dependence of the unit volume scattering cross section and, given an approximate description of the variation of cross section with scattering angle, the measurements may be used to verify the utility of the approximation.

The transmission loss is given in the absence of attenuation by the bistatic radar equation

$$\frac{P_r}{P_t} = \frac{1}{L} = \frac{G_1 G_2 \lambda^2}{(4\pi)^3} \int_{vol} g_1 g_2 \hat{u}_1 \cdot \underset{\approx}{\beta}_s \cdot \hat{u}_2 \, \frac{d\,vol}{r_1^2 r_2^2} \tag{1}$$

where

P_r = received power

P_t = transmitted power

L = transmission loss

λ = wavelength

G_1, G_2 = antenna gain for antennas 1 and 2, respectively

vol = volume of scatterers

g_1, g_2 = antenna gain function

$\hat{u}_1, \hat{u}_2$ = unit vectors representing the polarization behavior of antennas 1 and 2

$\underset{\approx}{\beta}_s$ = tensor scattering cross section per unit volume

r_1, r_2 = distances along the rays from the antennas to the elemental integration volume

$d\,vol$ = elemental integration volume.

Equation (1) is valid when attenuation does not occur in the scattering region or along the rays from the antennas to the scattering region. At frequencies for which attenuation is important, this effect should be included as was done in the computation procedure given in a previous report.[2] The Avon-to-Westford experiment was conducted at 4.515 GHz, a frequency at which attenuation effects may be neglected, and, for this reason, they will be ignored in the development of the equations for transmission loss estimation given here. It is further noted that the simplified procedure given in the previous report ignored polarization effects which are considered here.

Previous radar measurements[2] of scattering from both rain and thin turbulent layers have shown that the scatterers are not uniformly distributed through space but are confined in rather small volumes. This experimental fact allows one to simplify the bistatic radar equation by assuming that the important contributions to the integral in Eq. (1) come from the intersection of the limited rain or turbulent volume and the antenna pattern with the smallest main beam cross section at the volume. For interference problems, this assumption applies to most cases of main-beam main-beam coupling, and main-beam side-lobe coupling. For cases in which main-beam intersections occur and the intersection volume is smaller than the rain or turbulent volume, the intersection volume should be used. For side-lobe side-lobe coupling, only the limited rain or turbulent volume is considered. The case considered here is that in which the cross section of the main beam of antenna 1 in a plane through the volume of scatterers and normal to the beam is smaller than the cross section of the volume of scatterers in the same plane. The scattering volume then is defined by the main-beam cross section and the linear extent of the volume of scatterers along the beam (see Fig. 1). Equation (1) may also be further simplified, in this case, by assuming a constant scattering cross section per unit volume across the antenna beam.

Equation (1) then becomes

$$\frac{1}{L} = \frac{G_1 G_2 \lambda^2 g_2}{(4\pi)^3 r_2^2} \left[\int_0^{\Omega_m} g_1(\Omega)\, d\Omega\right] \left[\int_{r_1-(d/2)}^{r_1+(d/2)} \hat{u}_1 \cdot \underset{\approx}{\beta}_s(x) \cdot \hat{u}_2\, dx\right] \qquad (2)$$

where

Ω = solid angle coordinate of the volume, Ω_m is the value of Ω at the edge of the volume of scatterers

x = distance along the ray from antenna 1

d = limited distance dimension of the volume of scatterers.

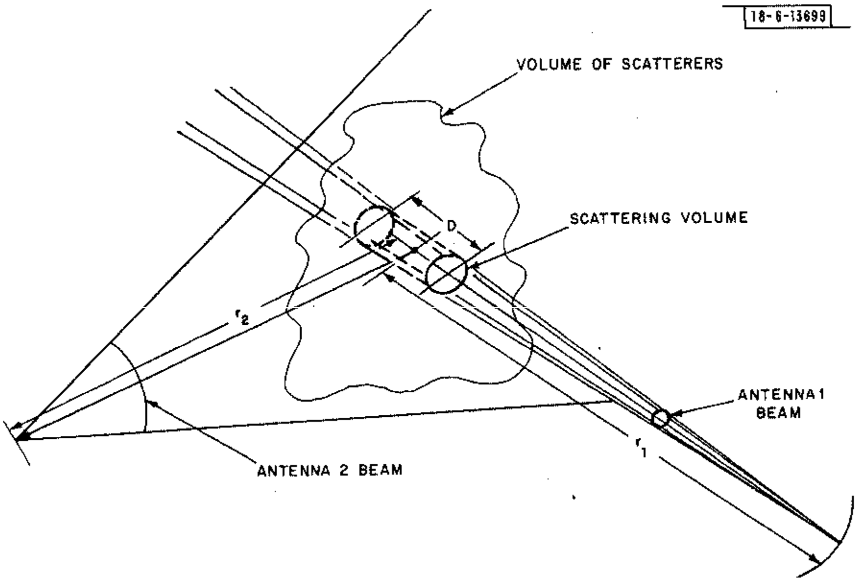

Fig. 1. Scattering geometry.

This may be rearranged further to

$$\frac{1}{L} = \frac{G_2(\hat{r}_2)\,\lambda^2 G_1 \Lambda \hat{u}_1 \cdot \underset{\approx}{\beta}_S \cdot \hat{u}_2}{(4\pi)^3 r_2^2} \tag{3}$$

where

$$\Lambda = D \int_0^{\Omega_m} g_1(\Omega)\, d\Omega$$

$$D = \frac{\int_{r_1-(d/2)}^{r_1+(d/2)} \hat{u}_1 \cdot \underset{\approx}{\beta}_S(x) \cdot \hat{u}_2\, dx}{\hat{u}_1 \cdot \underset{\approx}{\beta}_S(r_1) \cdot \hat{u}_2}$$

$$G_2(\hat{r}_2) = G_2 g_2 \quad .$$

With the assumptions made above, the expression for the integral over the antenna pattern is a known function and the values $\underset{\approx}{\beta}_S(r_1)$ and D must be determined from the distribution of scatterers in space. For the estimation of the statistics of transmission loss, the statistics of $\underset{\approx}{\beta}_S$ and D must be determined. For future reference, Eq. (3) will also be re-expressed as

$$\frac{1}{L} = C_B \frac{G_2(\hat{r}_2)\,\hat{u}_1 \cdot \underset{\approx}{\beta}_S \cdot \hat{u}_2 D}{r_2^2} \tag{4}$$

where $C_B = [\lambda^2 G_1/(4\pi)^3] \int_0^{\Omega_m} g_1(\Omega)\, d\Omega$ = a constant for a particular antenna and frequency.

Equation (1) may also be simplified for application to the radar problem. In this case, antennas 1 and 2 are the same and the bistatic scattering cross section per unit volume for a 180° scattering angle is used:

$$\frac{P_r}{P_t} = \frac{G_1^2\lambda^2}{(4\pi)^3}\int_{vol} g_1^2\beta_B \frac{d\ vol}{r_1^4} \qquad (5)$$

where $\beta_B = \hat{u}_1 \cdot \underset{\approx}{\beta}_s \cdot \hat{u}_1$ for 180° scattering angle. By using the assumption that the cross section of the main beam in a plane normal to the beam at the volume of scatterers is smaller than the cross section of the rain or turbulent volume, this equation may be simplified to

$$\frac{P_r}{P_t} = C_R \frac{\beta_B D}{r_1^2} \qquad (6)$$

where

$$C_R = \frac{\lambda^2 G_1^2}{(4\pi)^3}\int_0^{\Omega_m} g_1^2(\Omega)\ d\Omega \quad .$$

For a pulsed radar, d is the width of a range resolution cell or range box and r_1 is the distance to that cell.

Simultaneous measurements of $1/L$ or P_r/P_t using both bistatic scattering and radar systems provide measurements of β_B and $\hat{u}_1 \cdot \underset{\approx}{\beta}_s \cdot \hat{u}_2 D$. When the radar and antenna 1 of the bistatic system are colocated, measurements of the ratio of $\hat{u}_1 \cdot \underset{\approx}{\beta}_s \cdot \hat{u}_2 D$ to $\beta_B D$ may be made by integrating the scattering cross section along the radar beam. These values then do not depend on the width of either the radar resolution cell or of the volume of scatterers. The measured ratios may then be compared with the ratios predicted for particular scattering mechanisms to provide a check of the precision of the approximate descriptions of the scattering process. When the radar and bistatic scattering systems operate at different frequencies, the frequency dependence of the scattering process may also be checked.

The transmission loss estimation equations are complete when the bistatic cross section per unit volume is specified. For rain, Rayleigh scattering theory is normally used to describe the scattering process in the centimeter wavelength region. By using Rayleigh theory,[5]

$$\underset{\approx}{\beta}_s = (\hat{a}_1 \cos^2\varphi\hat{a}_2 + \hat{b}_1\hat{b}_2)\ \frac{\pi^5 Z|\kappa|^2}{\lambda^4} \qquad (7)$$

where

Z = sum of the sixth powers of raindrop diameters

$\kappa = (\epsilon - 1)/(\epsilon + 2)$, ϵ = dielectric constant for water

φ = scattering angle

$\hat{a}_1, \hat{a}_2$ = unit vectors in the plane of scattering normal to the ray from the antenna to the scatterer

$\hat{b}_1, \hat{b}_2$ = unit vectors normal to the plane of scattering.

The plane of scattering is defined as the plane containing the two antennas and the scattering volume. Computations of $|\kappa|^2$ using the dielectric constant given by Grant, et al.[6] show that $|\kappa|^2$ is weakly frequency dependent and in the centimeter region is approximately 0.93. Equations (4) and (7) may be combined to yield

$$\frac{1}{L} = A_R G_2(\hat{r}_2)\, u_1 \cdot (\hat{a}_1 \cos^2 \varphi a_2 + \hat{b}_1 \hat{b}_2) \cdot \hat{u}_2 \frac{ZD}{r_2^2} \tag{8}$$

where

$$A_R = \frac{\pi^2 |\kappa|^2}{64\lambda^2} G_1 \int_0^{\Omega_m} g_1(\Omega)\, d\Omega \quad .$$

By letting Z be expressed in mm^6/m^3, r_1 and D in kilometers, and λ in centimeters,

$$A_R = \frac{\pi^2 |\kappa|^2}{64\lambda^2} G_1 \int_0^{\Omega_m} g_1(\Omega)\, d\Omega \cdot 10^{-17} \quad . \tag{9}$$

For thin turbulent layers, the scattering cross section is given by[7]

$$\underset{\approx}{\beta}_s = (\hat{a}_1 \cos^2 \varphi \hat{a}_2 + \hat{b}_1 \hat{b}_2) \frac{0.378 C_n^2}{\lambda^{1/3} (\sin \frac{\varphi}{2})^{11/3}} \tag{10}$$

where C_n^2 = the structure constant, a meteorological parameter that describes the intensity of random fluctuations of the index of refraction in the inertial subrange. Equations (4) and (10) may be combined to yield

$$\frac{1}{L} = A_T G_2(\hat{r}_2)\, \hat{u}_1 \cdot (\hat{a}_1 \cos^2 \varphi \hat{a}_2 + \hat{b}_1 \hat{b}_2) \frac{C_n^2 D}{r_2^2} (\sin \frac{\varphi}{2})^{-11/3} \tag{11}$$

where

$$A_T = \frac{0.378 \lambda^{5/3}}{(4\pi)^3} G_1 \int_0^{\Omega_m} g_1(\Omega)\, d\Omega \quad .$$

By letting C_n^2 be expressed in $m^{-2/3}$, r_2 and D in kilometers, and λ in centimeters,

$$A_T = \frac{1.76 \lambda^{5/3}}{(4\pi)^3} G_1 \int_0^{\Omega_m} g_1(\Omega)\, d\Omega \cdot 10^{-7} \quad . \tag{12}$$

Equations (8), (9), (11), and (12) comprise the approximate description of the transmission loss due to rain and thin turbulent layer scatter.

III. THE AVON-TO-WESTFORD BISTATIC SCATTER SYSTEM

Measurements of transmission loss were made on a 143-km scatter path between a transmitter in Avon* and the Westford Communications Terminal. The scatter measurement system parameters are summarized in Table I. The system operated at a frequency of 4.515 GHz, with the transmitter mounted in a transportable terminal. Two transmitting antennas were available, a 4-foot parabola and a standard gain horn; they were mounted on top of a van (see Fig. 2) and were manually switch selected and steered by an operator in the van. The receiver system used

*Site provided courtesy of Station WTIC, Hartford, Connecticut.

TABLE I

AVON-TO-WESTFORD BISTATIC SCATTER SYSTEM

Frequency	4.515 GHz (6.644-cm wavelength)
Antenna 1	60-foot with Cassegrainian feed
Gain antenna 1	55.5 ± 0.7 dB
Beamwidth antenna 1	0.2° between half-power points
Polarization antenna 1	Vertical
Antenna 2	4-foot parabola with prime focus feed Standard gain horn
Gain antenna 2	32.8 ± 0.3 dB for 4-foot 18.1 ± 0.1 dB for horn
Beamwidth antenna 2	3.5° for 4-foot 22° for horn
Polarization antenna 2	Vertical
Transmitter power	Variable 1 W to 1 kW
Transmitted signal	CW with frequency stability of 1 part in 10^{10} per day
Receiver	Phase lock
Receiver bandwidth	560 and 2880 Hz
Receiver noise temperature	~1000°K (with image rejection filter)
Maximum measurable transmission loss	190 dB
Path length	143 km
Data processing	Received signal AGC voltage and local oscillator frequency sampled 20 times per second
Minimum detectable Z_e	−5 dBZ* at midpath on great circle plane
Minimum detectable C_{ne}^2	10^{-18} $m^{-2/3}$ at midpath on great circle plane

*dBZ specifies dB relative to $Z_c = 1$.

Fig. 2. Transportable terminal at Avon, Connecticut.

Fig. 3. Millstone Hill and Westford sites.

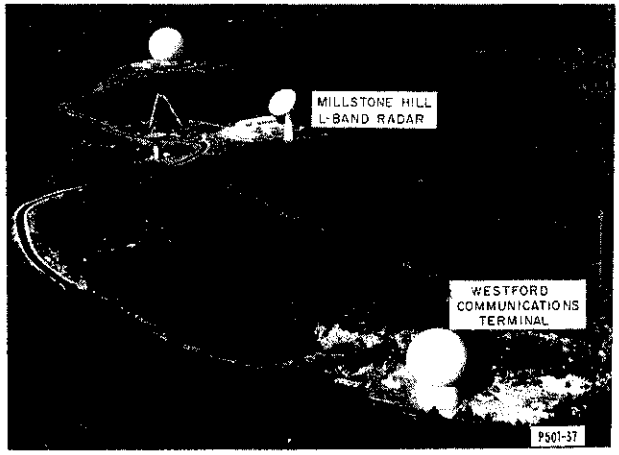

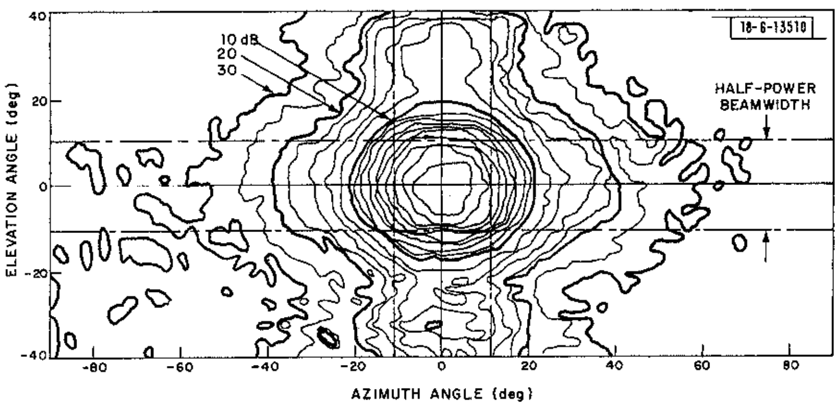

Fig. 4. Contour plot — standard gain horn mounted on 4-foot antenna as used at Avon. Frequency: 4.515 GHz; polarization: vertical; gain: 18.1 dB. (Cross polarized component <27 dB for entire pattern.)

the 60-foot Westford Antenna which could be slaved to the Millstone Hill radar antenna for simultaneous pointing of both systems (see Fig. 3). The transmit and receive antennas were vertically polarized.

The transmitting antennas were both attached to a manually controlled azimuth, elevation mount with the standard gain horn mounted just above the 4-foot antenna. Contour patterns of each of the antennas when mounted together as used in the experiment are given in Figs. 4, 5, and 6. The patterns and gain measurements were made at the Antenna Test Range operated by Lincoln Laboratory.[8] The Westford Antenna system was modified to take a 4.515-GHz horn feed in place of the normal X-band tracking feed (see Ref. 9 for a description of the X-band system). Pattern measurements of the Westford 4.515-GHz system were made using a transmitter on the Groton Fire Tower which served as the boresight tower. The transmitter was located 5.2 km ($\mathfrak{D}^2/\lambda$ = 5.0 km where $\mathfrak{D}$ is the antenna diameter) from the antenna. Antenna gain was measured by both the substitution method and the direct transmission loss method using the source on the

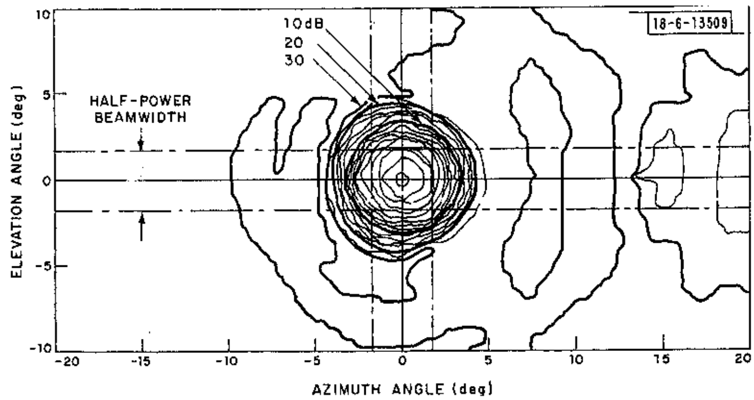

Fig. 5. Contour plot – 4-foot antenna with standard gain horn mounted on top as used at Avon. Frequency: 4.515 GHz; polarization: vertical; gain: 32.8 dB.

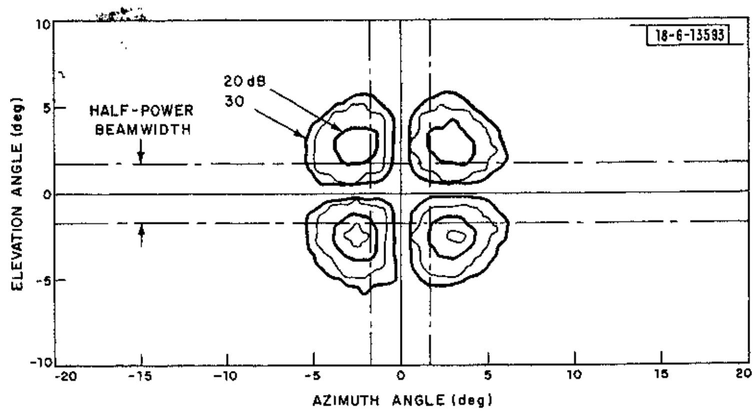

Fig. 6. Contour plot – 4-foot antenna with standard gain horn mounted on top as used at Avon. Frequency: 4.515 GHz; polarization: crossed.

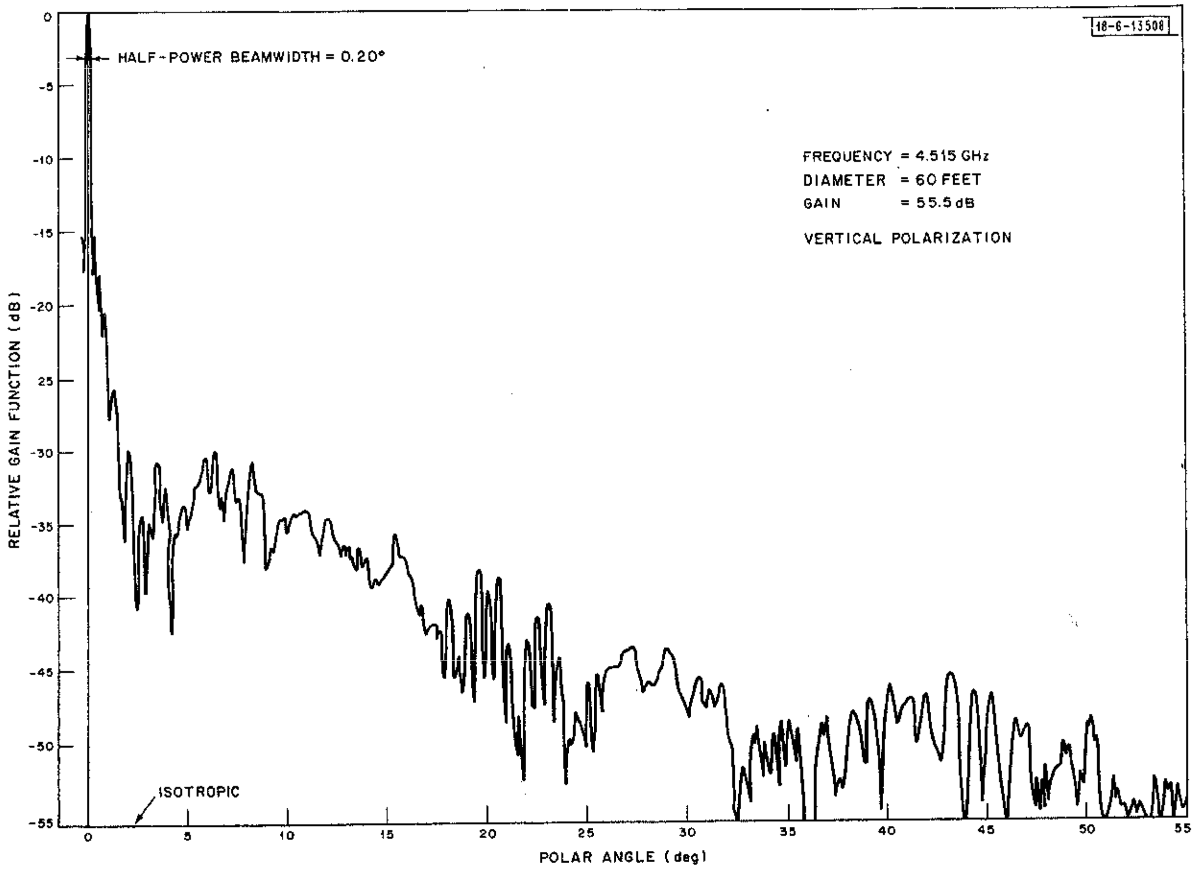

Fig. 7. Envelope of principal plane patterns for Westford communications antenna.

fire tower with a standard gain horn and, for the substitution measurement, a 4-foot gain standard antenna. The gain standard and transmitter antennas were calibrated by comparison with a reference standard gain horn at the Antenna Test Range. Both techniques were used because an obstacle was present in the 14th Fresnel zone at a distance of 0.7 km from the boresight tower. The obstacle was at a 0.3° polar angle from boresight as measured at the Westford Antenna or at the peak of the first side lobe (see Fig. 7). At this angular distance, the signal reflected from the obstacle will be resolved as a separate source with the 60-foot antenna, but will not be resolved using the substitution standard. By using the difference between the upper and lower elevation side lobes and the level of the lower side lobe as measured employing the source on the boresight tower, the signal as reflected by the obstacle is estimated to be more than 16 dB below the boresight line-of-sight power level. This implies that the error in the substitution method measurement due to the pattern range is less than ±1.3 dB, and for a direct transmission loss measurement it is less than ±0.2 dB. By utilizing these values and the maximum error estimates for component mismatch, for the uncertainty in component values, and for the instrument reading errors, the maximum error found in the direct transmission loss measurement is ±0.7 dB and in the substitution method measurement is ±1.7 dB. The difference between the averages of several measurements using each of the techniques was 0.3 dB. The resultant antenna gain as measured employing the average of the direct transmission loss measurements is estimated at 55.5 ± 0.7 dB. Although an attempt was made to measure the cross polarized pattern of the Westford Antenna, it could not be measured with the available equipment. The antenna has an $f/\mathfrak{D}$ ratio of 0.30 where f is the focal distance and, with a multiplication factor of 14.3 for the Cassegrainian system, the cross polarization side lobes are conservatively estimated to be more than 25 dB below the peak antenna gain.[10]

The measured patterns were used to estimate the percent included power as a function of polar angle as shown in Fig. 8. The computation of percent included power was made by azimuthally averaging the measured principal plane patterns then numerically computing the integral of the antenna gain function over the cone of solid angles out to the polar angle given. A percent value was given to the result of the integration by comparing the result with the known value for

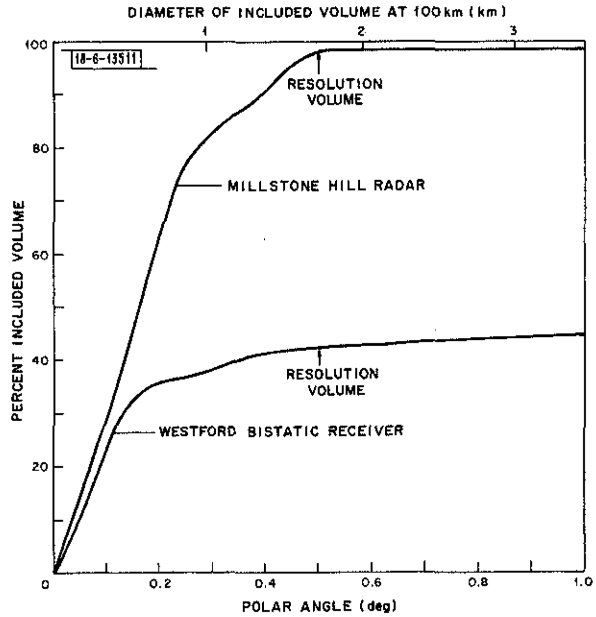

Fig. 8. Percent included power for Westford and Millstone Hill antennas.

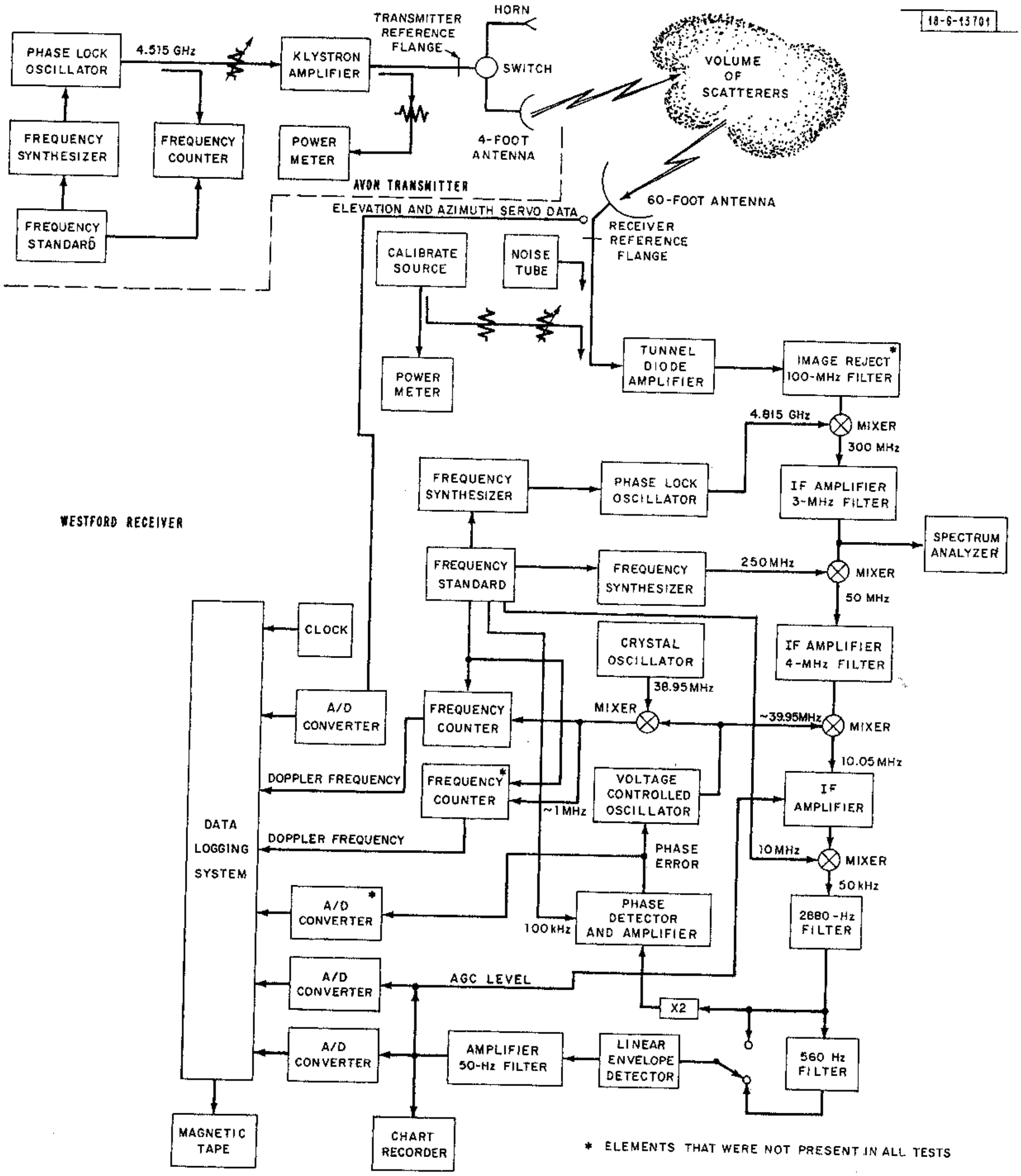

Fig. 9. Block diagram, Avon-to-Westford bistatic scatter system.

the integral of the gain function over 4π steradians. The value of Ω used in the evaluation of the integral is $2\pi(1 - \cos\gamma)$ where γ is the polar angle marked on the figure. Ω_m was selected so that an error of less than 0.3 dB in the value of the integral would occur when the volume of scatterers ranged from 1.1 to 10 km across the beam at a distance of 100 km. Using this value,

$$G_1 \int_0^{\Omega_m} g_1(\Omega)\, d\Omega = 5.1 \pm 1.1$$

where the accuracy estimate includes a maximum uncertainty of ±0.7 dB in the estimate of the antenna gain measurement and a ±0.1-dB estimate of the pattern integration error. It is noted that the value for the integral is 0.3 dB higher than would be obtained using the Gaussian beam shape approximation and 1.8 dB higher than for the simple model pattern with no response outside and unity response within the half-power polar angle.[2]

The transmitter system (see Fig. 9) used a Varian VA-888E klystron amplifier to produce a continuous wave (CW) signal that could be varied between 1 W and 1 kW at the reference flange of the transmitting antenna. The klystron was driven by an oscillator that was phase locked to the 44th harmonic of a tone from a Hewlett-Packard Model 5105-A Synthesizer synchronized with a General Radio Crystal Frequency Standard Type 1115-B. The transmitted radio frequency signal (RF) was continuously monitored using both a frequency counter and a power meter which was calibrated to read the transmitted power referenced to the transmit antenna flange. The transmit power level was varied manually using a variable attenuator between the oscillator driver and the klystron amplifier. The high voltage was also varied to ensure a good transmitter output signal-to-noise ratio. The van was air conditioned to provide temperature control for all transmitter components. An operator was present during each experiment to position the antenna, change transmitter power, and monitor the operation of all components.

The receiver system used a tunnel diode RF amplifier with a 5-dB noise figure. The received signal was translated through three intermediate frequency (IF) stages to a final 50-kHz IF. Detection was performed using either a 560- or a 2880-Hz predetection filter and a linear envelope detector in an AGC loop with a 50-Hz post-detection bandwidth. AGC voltage was sampled without further integration, quantized, and recorded digitally at a 20-times-per-second rate. The first local oscillator was similar to the oscillator used to drive the transmitter. The receiver was of the phase lock type with a local oscillator controlled by the phase lock loop. This oscillator was monitored using an interval counter that provided an estimate of the received frequency with 1-Hz accuracy every 50 msec. The frequency was recorded digitally at the 20-sample-per-second rate to provide a measurement of the doppler shift of the received signal. A second frequency counter was also used that provided a 1-sec average frequency estimate. All other local oscillators were synchronized to the frequency standard. By using the doppler measurement system and thin turbulent layer scatter along the great circle path, the relative drift of the transmitter and receiver frequency standards was measured to be on the order of 1 Hz per day at RF.

The digital tape recording system sampled the antenna position and station clock 20 times per second in addition to recording the doppler shift measurements and AGC level. The AGC level was recorded using two 6-bit analog-to-digital converters which were operated so that together they covered a 50-dB range of received signal levels. The AGC characteristic was logarithmic over a 60-dB range; however, the higher signals tended to saturate and the lower signals were masked by noise providing a measurement range of 30 dB. The dynamic measurement range

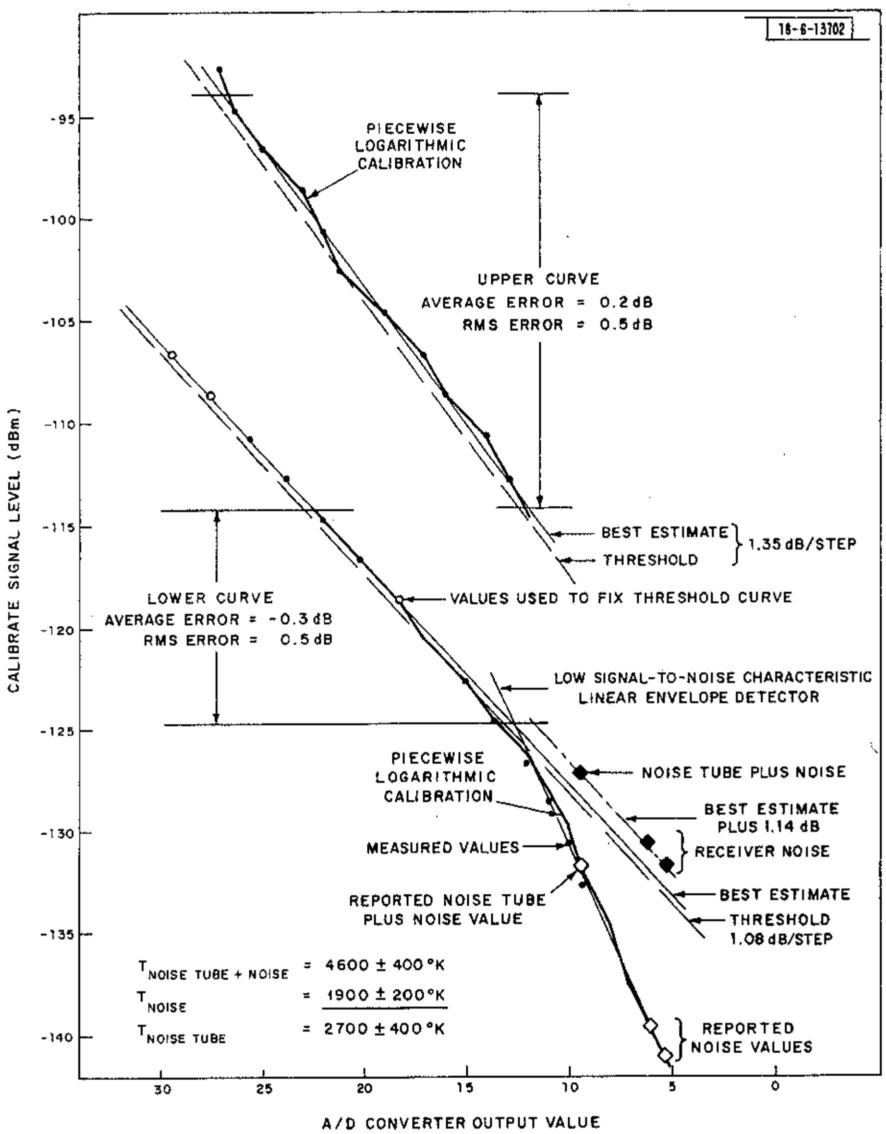

Fig. 10. Calibration curve for Westford recording system. 29 July 1970, 2310 to 2355 GMT; 2880-Hz bandwidth; no image rejection filter.

of the bistatic scattering system was extended from 30 to 60 dB by varying the transmitter power. The converters were adjusted so that the logarithmic AGC voltage was sampled in approximately 1.3-dB steps in the high-level channel and 1.0-dB steps in the low-level channel. Receiver calibrations were performed at the beginning of each tape or approximately once every 3 hours. The calibrations were performed by coupling an RF signal of precisely known amplitude into the waveguide ahead of the tunnel diode amplifier (receive antenna reference flange). Two calibrations were performed – one using a tone which was varied over a 50-dB range in 2-dB steps and the other using a noise tube of known temperature.

Data were recovered from the digital magnetic tapes using the Laboratory computer system. The data recovery program was calibrated using the recorded calibration tones. One hundred sample data points were averaged at each of the 26 calibration levels. Logarithmic interpolation was used between the levels to generate the calibration curve used in the data processing (see Fig. 10). The calibrate tones used to generate the upper curve had a high signal-to-noise ratio and the values tended to lie between the thresholds of the recording levels. Only the threshold values, however, are reported. The straight line which reproduces the logarithmic characteristic of the AGC circuit is plotted through the lower threshold values. This line was passed through the next higher threshold value when the averaged calibration values were between the threshold values. The slope was adjusted so that the line was between the measured threshold value and the next higher value for all samples below the saturation level. For fluctuating signals typical of rain and thin layer scatter, the sample points will span several measurement steps. If the density of sample points within a measurement interval is assumed to be uniform, the best estimate calibration curve lies one-half the width of the quantization step above the threshold value. The best estimate curve on Fig. 10 was produced by shifting the threshold curve one-half quantization step. This curve was used to compute the average calibration error. The *rms* calibration error was calculated by taking the square root of the sum of the variances due to the wander of the piecewise logarithmic calibration curve about the best estimate curve, and the variance due to the assumed uniform density of sample points across a measurement interval. Average errors obtained in this manner were used to correct the averages calculated by the computer program using the piecewise logarithmic calibration curve. The calibration curves still may have an average error as large as 0.5 dB due to an uncertainty in the amplitude of the calibrate tone and in the position of the best estimate curves.

The lower best estimate curve was generated in the same manner. For this channel, the calibrate tone becomes masked by the noise as it decreases in amplitude. The small signal-to-noise ratio characteristic of the linear envelope detector is shown as the straight line with twice the slope of the best estimate curve.[11] A check on the slope of the best estimate curve was provided by comparing the slope of the low signal-to-noise curve with that of the measured points. The calibration curve deviates from the measured points in the noise dominated region due to the use of signal-plus-noise in the computer calibration routine. The best estimate curve was also checked by comparing the measured noise tube temperature with its known value. Temperature was measured using the best estimate curve. Samples of noise tube plus receiver noise, and of receiver noise were processed through the data logging system and the computer program. In Fig. 10, 5-sec averages are shown as open diamonds. The analog-to-digital converter output value was determined from the calibration curve and used to set the measured value on the best estimate curve. Since the correlation time for the noise is small in comparison with the post-detection filter bandwidth, an additional 1.14-dB correction must be added to the best estimate

TABLE II

AVON-TO-WESTFORD BISTATIC SCATTER SYSTEM MEASUREMENT ACCURACY

Element in Block Diagram (Fig. 9)	Absolute Accuracy Maximum (dB)	Calibration Repeatability Maximum (dB)	Volume Location Fluctuation		Sample Fluctuation RMS (dB)
			Main Beam RMS (dB)	Far Side Lobe RMS (dB)	
Transmitter					
Power monitor	0.2*	0.1	–	–	0.1
Antenna					
Horn	0.1	–	0.1	3.0	–
4-foot	0.3	–	0.1	3.0	–
Receiver					
Antenna gain	0.7	–	–	–	–
Antenna pattern integral	0.1	–	0.3	0.3	–
Noise tube	0.3	–	–	–	–
Calibrate Source					
Power monitor	0.2*	0.1	–	–	–
Attenuator setting	–	0.1	–	–	–
Analog-to-digital converter	–	0.3	–	–	0.6†
Estimation error for Rayleigh process	–	–	–	–	1.6‡
Receiver gain drift	–	0.2	–	–	–
Transmission Loss Measurement (P_t/P_r)	0.4	0.8	–	–	1.7
Measurement of $\hat{u}_1 \cdot \underset{\approx}{\beta}_s \cdot \hat{u}_2 D$					
Horn	1.3	0.8	0.3	3.0	1.7
4-foot	1.5	0.8	0.3	3.0	1.7

* Includes line loss error (maximum) used to transfer readings to reference points.

† Upper calibration curve.

‡ Five independent samples.

curve value. The resultant noise measurements are shown as solid diamonds on the best estimate plus 1.14-dB curve in Fig. 10. Temperatures corresponding to the best estimate value are also given in Fig. 10 where the error bounds are one standard deviation value due to quantization error. The noise tube temperature agrees with the expected value of 2200° ± 200°K for the noise tube when the image rejection filter is not used.

The computer analysis program decodes the input tapes and assigns each recorded AGC level the received signal value determined using the piecewise logarithmic calibration tables. The outputs of both AGC channels are combined by selecting the upper channel when it equals or exceeds a preset threshold, and selecting the lower channel when the upper channel value is below the threshold value. The received power value is then linearly averaged for 1 sec to produce an estimate of the received signal strength. The logarithm of the estimate is computed and recorded on tape for further processing. The computer program linearly averages the received power and, if the correlation time for rain or thin turbulent layer scatter is long in comparison with 20 msec, the 1-sec average of the fluctuating target is correct. If the correlation time for the scattering process is short in comparison with 20 msec, the 50-Hz post-detection filter integrates the amplitude of the received signal and the estimate of received power is 1.14 dB low (see Ref. 12). For processes with intermediate correlation times, the estimate of the received power will be between the correct value and 1.14 dB low.

In the estimated value of $\hat{u}_1 \cdot \underset{\approx}{\beta}_s \cdot \hat{u}_2 D$, the average error is less than 1.0 dB using the horn antenna or 1.2 dB using the 4-foot antenna for a process with a long correlation time, such as great circle path thin turbulent layer scatter. The absolute error budget is given in Table II. The average error budget holds when the receiver calibration is corrected as discussed above and the results of sets of measurements with independent calibrations are averaged. For a single set of scans or measurements with one calibration, the maximum uncertainty in the average of $\hat{u}_1 \cdot \underset{\approx}{\beta}_s \cdot \hat{u}_2 D$ is the sum of the accuracy and repeatability values in Table II, or 1.8 dB for the horn and 2.0 dB for the 4-foot antenna. The rms error in $\hat{u}_1 \cdot \underset{\approx}{\beta}_s \cdot \hat{u}_2 D$ is caused by level-to-level calibration uncertainties, the variance due to the relatively large analog-to-digital converter quantization steps and transmitter power fluctuations, transmitter antenna pointing errors, variations in the size of the volume of scatterers, and fluctuations in the scattering process. For a process with a 200-msec correlation time and approximately five independent samples in the 1-sec averaging period, the rms error is 1.7 dB for volumes within the transmit antenna main beam and first few side lobes. For scatter volumes in the far side lobes of the transmit antenna, the rms error is approximately 3 dB.

The Avon-to-Westford scatter path is depicted in Figs. 11 and 12. The terrain between the terminals is low lying, with hills generally below 1000 feet high. On this path, terrain diffraction and ducting tend not to be problems due to the generally uniform height and irregularity of the hills. The Westford Antenna has a relatively clear horizon above 0.4° elevation angle in the azimuth angle sector 140° to 310° available for the measurements. Pointing of the Westford Antenna was limited to this azimuth sector by the cable-wrap design. At azimuths between 243° and 249° and between 280° and 310°, a ridge of low mountains varying from 1500 to 2300 feet high at an approximate range of 40 km provided masking at elevation angles below 1°. The foreground at Avon is depicted in Fig. 13. The foliage extended to elevation angles between 0.7° and 4° in the sector shown, and to 60° behind the van as shown in Fig. 2. The Avon transmitter site was on one of the hills of the Talcott Mountains, and the solid earth was generally below 0.5° in all directions.

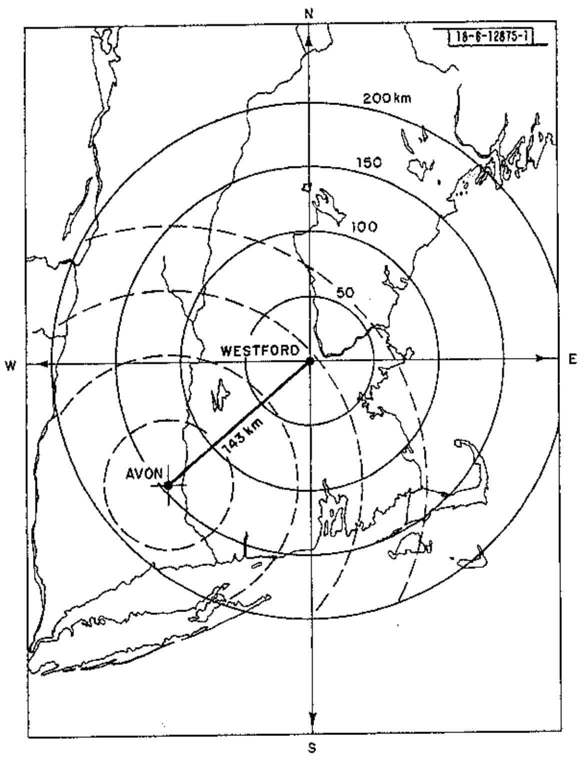

Fig. 11. Avon-to-Westford scatter path.

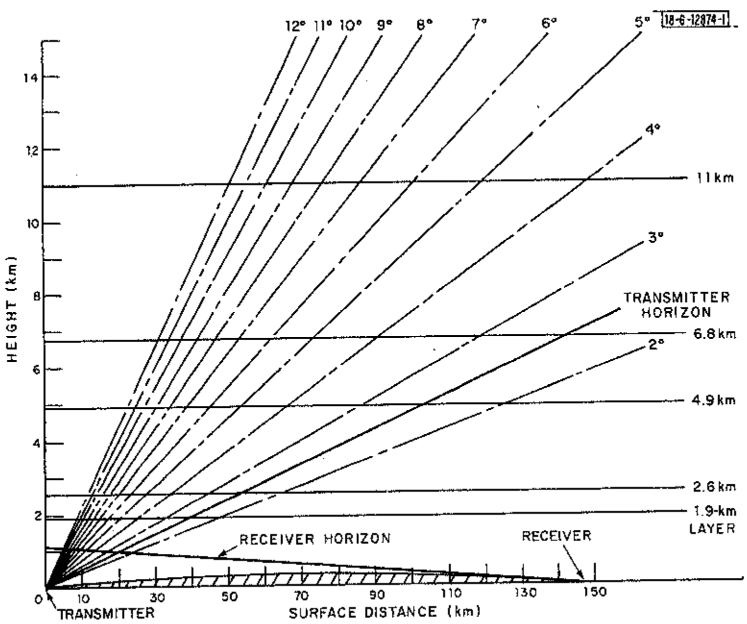

Fig. 12. Great circle plane cross section for Avon-to-Westford 143-km path.

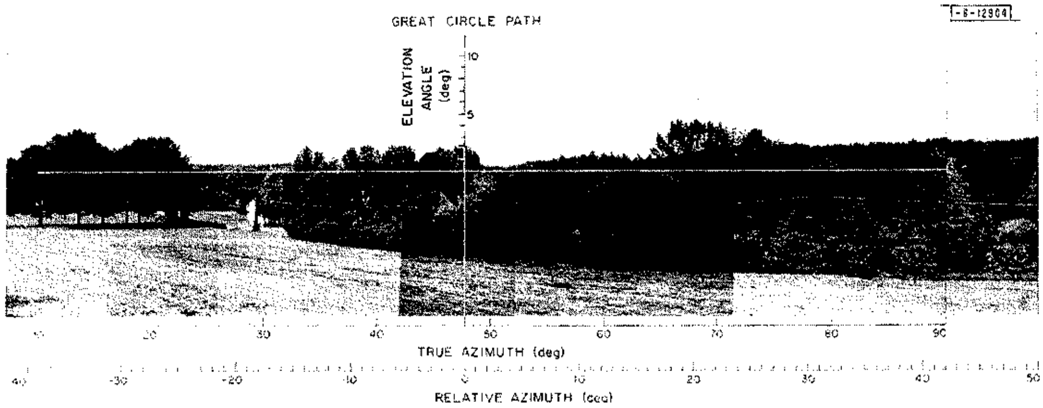

Fig. 13. Foreground at Avon, Connecticut.

IV. THE MILLSTONE HILL L-BAND RADAR

Measurements of the backscatter cross section per unit volume of rain or thin turbulent layers were made using the Millstone Hill L-band radar; the parameters of the radar are summarized in Table III. The radar used an 84-foot antenna that was computer controlled. This antenna was used to servo control the Westford Antenna. The pointing accuracies of both antennas are better than 0.05° and, with the relatively larger resolution beamwidths (see Fig. 8), pointing errors for either Westford or Millstone Hill may be ignored. Antenna gain was measured using radio star flux measurements. In Eq. (6), the integral over the square of the antenna gain function was determined using measured antenna patterns. The composite envelope of the principal plane patterns for both transmission and reception as measured using a linearly polarized source on Pack Monadnock Mountain is given in Fig. 14. The transmitter was at a distance of 42 km ($\mathfrak{D}^2/\lambda$ = 2.8 km). Both horizontal and vertical polarization measurements were included in the patterns. By using the measured patterns and independent gain measurements,

$$G_1^2 \int_0^{\Omega_m} g_1^2(\Omega)\, d\Omega = (2.1 \pm 4) \times 10^5$$

where the accuracy estimate includes a maximum uncertainty of 0.3 dB in the estimate of the antenna gain, and 0.1 dB for the pattern integration.

The radar system used a klystron transmitter and low-noise parametric receivers (see Fig. 15). Two linear receiver systems were used with line losses selected so that an 80-dB dynamic range could be obtained. The radar was operated with a 3.3-MW peak-power pulse, a 12.4-μsec pulse length, a 120-pulse-per-second repetition rate, and computer sampling on every sixth pulse. Matched filters were used on both the sine and cosine channels of each receiver system. The output from each of the filters was sampled at a 100-kHz rate using 10-bit analog-to-digital converters and stored in the SDS 9300 computer. Data were stored in 120 range boxes of 1.5-km (10-μsec) extent. The signals were square law detected and incoherently integrated in the computer. Fifty independent samples were integrated which, for a Rayleigh process such as rain scatter, resulted in an rms error of 0.7 in the estimate of the backscatter cross section per unit volume.

The radar system performance was continuously monitored. Transmitter power was recorded on a strip chart and typically varied by less than ±0.1 dB for a 6-hour run. The receiver system

TABLE III

MILLSTONE HILL L-BAND RADAR

Frequency	1.295 GHz (23.2-cm wavelength)
Antenna	84-foot parabola with Cassegrainian feed
Antenna gain	46.7 ± 0.3 dB ("new" subreflector)
Beamwidth	0.7° between half-power points
Polarization	Right-hand circular transmitted Left-hand circular received
Transmitted power	3.3-MW peak (continuously monitored)
Pulse length	12.4 μsec
Pulse repetition rate	120 per second
Receiver bandwidth	80.5 kHz (12.4-μsec matched predetection filter)
Data processing	Analog-to-digital conversion of IF sine and cosine channels every 10 μsec
Computer sampling rate	20 per second
Detection	Square law by computer operations
Dynamic range	80 dB accomplished by combining the output from two receivers
System noise temperature	280°K (includes atmospheric and ground effects averaged over 0° to 30° elevation angle)
Overall system line losses	2.8 dB for receiver 1 43.5 dB for receiver 2
Matched filter processing loss	1.1 dB
Single-pulse Z_e value for unity signal-to-noise ratio	−30 dBZ at 100 km
Single-pulse C_{ne}^2	$10^{-16} m^{-2/3}$ at 100 km

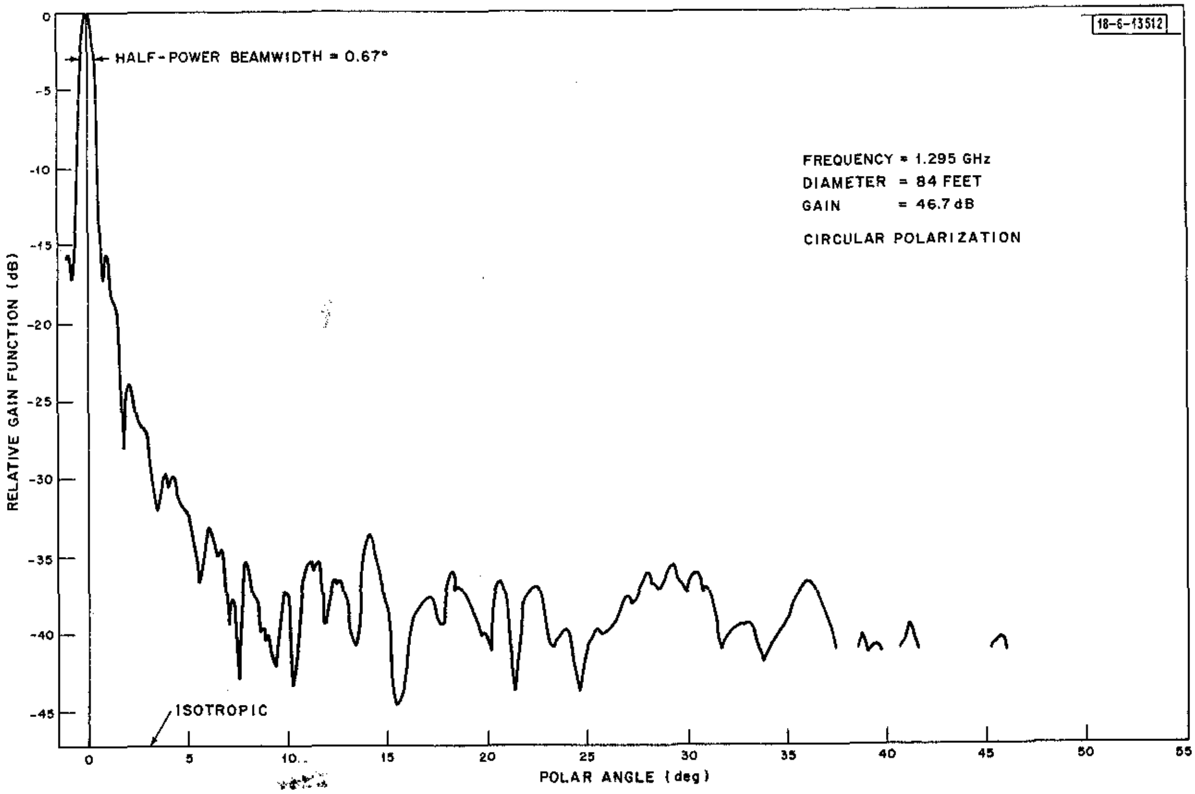

Fig. 14. Envelope of principal plane patterns for both transmission and reception for Millstone Hill L-band radar antenna.

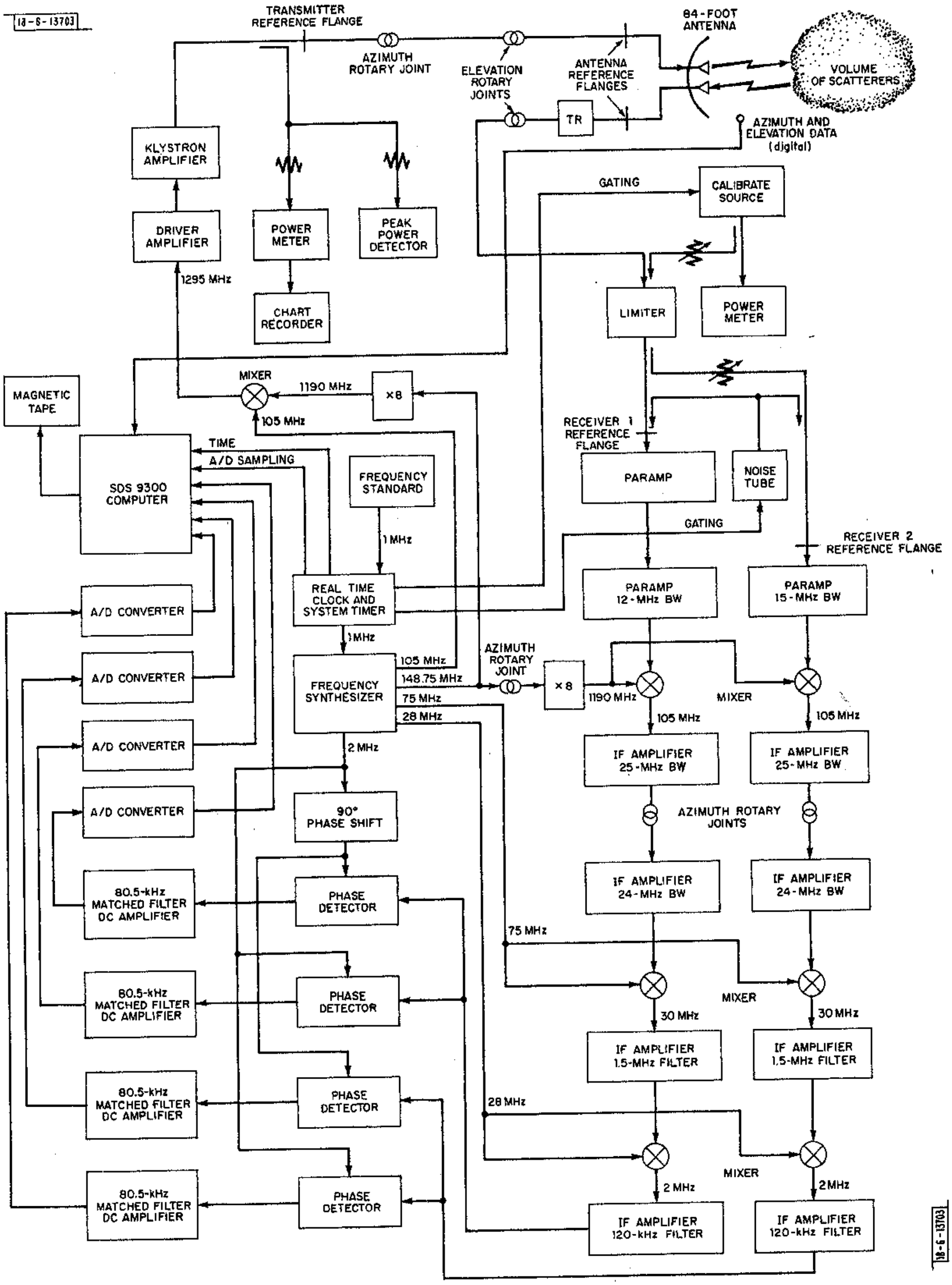

Fig. 15. Block diagram, Millstone Hill L-band radar.

was calibrated continuously using a pulsed noise tube of known temperature. Twenty-five consecutive samples of receiver noise and 25 samples of noise tube plus receiver noise were averaged for each of the 50 pulses being integrated. The noise tube and noise measurements were made at ranges in excess of 600 km where no radar targets are expected. Ionospheric echoes were not present due to the relatively low average power, low elevation angle, and the generally southerly azimuth directions used in the measurement program. The received signal strength for each radar return was estimated by subtracting the average noise value from the average signal-plus-noise value and scaling by the ratio of the known noise tube power to the value obtained by subtracting the average value of noise from the average noise-tube-plus-noise value. The computer program multiplied the estimate of the received signal power by the square of the range to the target and recorded it on magnetic tape. Calibration of the receiver was continuously monitored by gating on an RF tone of known amplitude for 12.4 μsec at the fourth-from-last range box and processing through the computer. Both the tone and noise tube calibrations were made from the same waveguide reference point at the input flange of each parametric amplifier (paramp). Typically, the receiver calibration varied by less than ±0.2 dB as measured by the fluctuations in the RF tone amplitude.

The absolute calibration of the radar system was made by combining the values of each factor in the radar equation. Table IV shows the error budget for the calibration. The maximum error for all the data is ±1.4 dB and for a single set is ±1.6 dB. An overall check on the system calibration was made by observing spheres of known cross section in orbit.* Measured cross sections were within 0.5 dB of the known values of the cross sections of the several spheres used. The sphere calibrations were made prior to the installation of the "new" subreflector. The gain with the "old" subreflector was measured both by radio star flux measurements and by the substitution method using a source on Pack Monadnock Mountain. The radio star flux measurements with the "new" subreflector provided a means of comparing the antenna gains before and after the subreflector change. This allows use of the sphere measurements in a separate calibration error determination. The sphere measurements are within the maximum bounds listed in Table IV. This overall system calibration checks every factor in the radar equation except the value of the integral of the square of the antenna gain function. The integral depends only upon the shape of the main lobe and first few side lobes of the antenna pattern and is known to within 0.1 dB. The maximum uncertainty in the absolute calibration of the radar for a volume target applies only when the volume target fills the beam. When the volume is less than the resolution volume (1.7 km across the beam at 100 km, and 1.9 km along the beam), the estimate of the peak cross-section value will be in error. When the data are used for comparison with measurements using the Avon-to-Westford bistatic scatter system, the resolution cell filling errors do not apply since the angular resolutions of both systems are nearly identical and range averaging of the radar data is performed in the comparison. The rms error in the estimate of the cross-section value is 0.7 dB for a Rayleigh process with a correlation time small in comparison with 50 msec.

Data recorded on magnetic tape were analyzed using the Laboratory computation facilities. The first stage of processing combined the output of both receivers. Output from the more sensitive receiver was used unless the received signals in both receivers were higher than four standard deviations of their respective receiver noises above the noise. When this received signal value condition was met, the output of the less sensitive receiver was used. The received

* U.S. Navy 14-inch-diameter calibration spheres, Space Track Object Nos. 900, 902, 1512 and 1520; 20-inch-diameter sphere, No. 2826.

TABLE IV

MILLSTONE HILL L-BAND RADAR MEASUREMENT ACCURACY

Element in Block Diagram (Fig. 15)	Absolute Accuracy Maximum (dB)	Calibration Repeatability Maximum (dB)	Sample Fluctuation RMS (dB)
Transmitter			
Power monitor*	0.2	0.1	0.1
Line loss	0.1	–	–
Antenna			
Transmit and receive gain	0.6	–	–
Pattern integration	0.1	–	–
Receiver			
Noise tube	0.3	0.1	–
Calibrate source*			
Power monitor	0.2	0.1	–
Attenuator setting	–	0.1	–
Line loss	0.1	–	–
Estimation error for Rayleigh process	–	–	0.7
Measurement of P_r/P_t	0.7	0.2	0.7
Measurement of β_B	1.4	0.2	0.7

**Includes line loss error (maximum) used to transfer readings to reference points.*

signal value was then scaled to units of mm^6/m^3 and reported as Z_e. Scaling constants were found by using Eqs. (6) and (7) and the parameters listed in Table IV.

V. COMPARISON ANALYSIS

The radar and bistatic scatter systems provide measurements of the backscatter cross section per unit volume and the bistatic scatter cross section per unit volume integrated over nearly identical angular regions. The radar reports the cross-section values integrated over a range cell; the bistatic system reports the cross-section values weighted by both the transmitter antenna pattern and the distance between the transmitter and scattering volume and integrated along the receiver beam. By suitable processing of the radar data, an estimate of the radar cross section for a weighted integration volume identical to the one for the bistatic scatter system can be calculated. With identical volumes, the ratio of the backscatter and bistatic scattering cross sections may be computed and compared with the value predicted by the approximate description used for the scattering process. A statistical description of the comparisons for each of the relevant scattering mechanisms (rain and turbulence) constitutes the results of the Avon-to-Westford experiment. The previous sections described the systems used to make the measurements; this section presents the details of the analysis programs used in processing the data to make the comparison.

The measurement program was conducted with both the radar and bistatic scatter systems observing the same volumes in space. To provide many independent measurements of the scattering process at different scattering angles, the Millstone Hill and Westford antennas were scanned in synchronism. The scanning nature of the experiment also insured that the most interesting phenomena would be observed. Two computer programs were used to process the measured data, as schematically shown in Fig. 16. The Westford data processing program extracted the measurements from the magnetic tapes generated at the site, averaged the data, assembled the data by scans, and wrote the averaged received signal level and antenna pointing angles on a

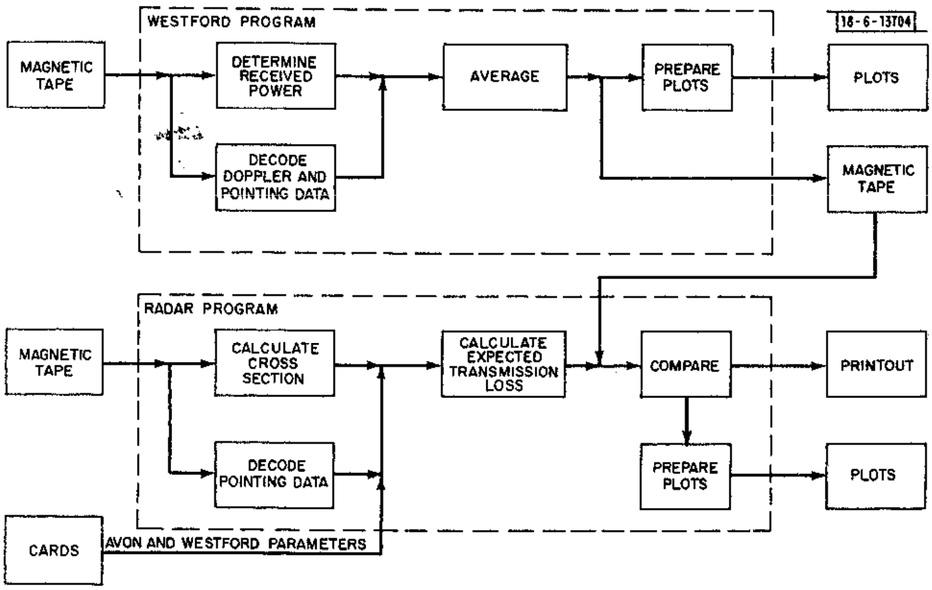

Fig. 16. Data processing block diagram.

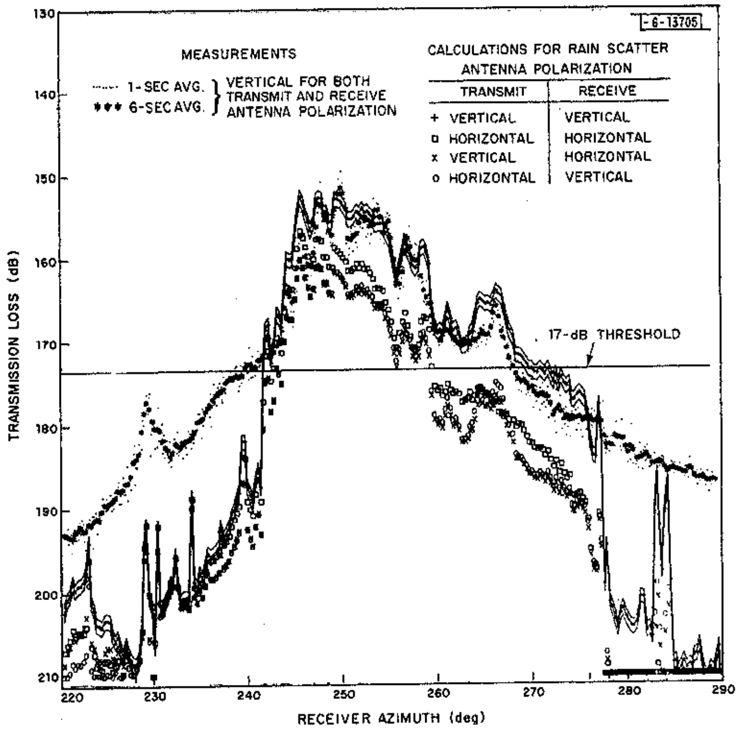

Fig. 17. Measured and calculated transmission losses due to rain. Westford: 1.5° elevation angle. Avon: 6° elevation angle; 23° azimuth; horn antenna.

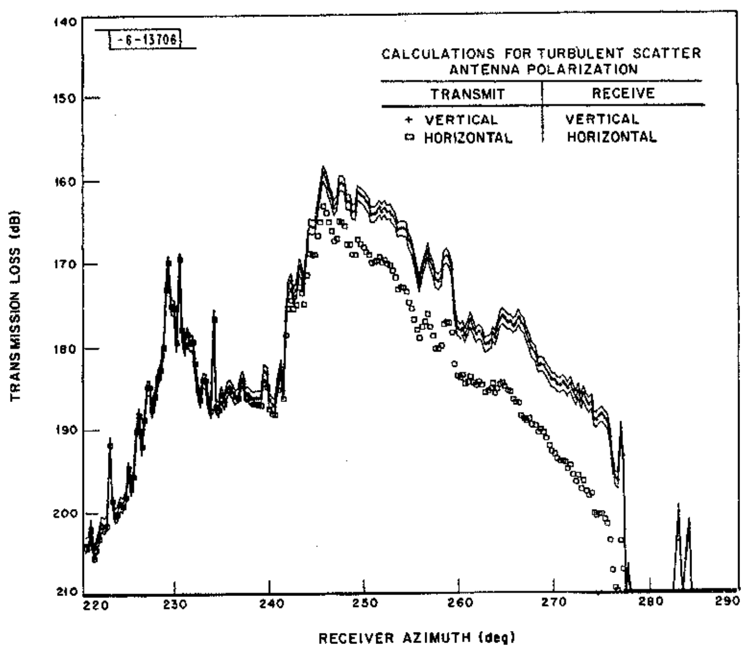

Fig. 18. Calculated transmission loss due to turbulence. Westford: 1.5° elevation angle. Avon: 6° elevation angle; 23° azimuth; horn antenna.

second magnetic tape. The second program – the radar data processing program – read the site tapes, converted the reported received power distance squared product into cross-section estimates, and assembled the data by scans. This program then computed the expected transmission loss value for the Avon-to-Westford measurements using Eqs. (6) through (12), read the tape generated by the Westford program, and used the data for comparison with the calculated values. Finally, this program plotted the measured and calculated values of transmission loss for each scan and prepared comparison tables for the ratio of calculated-to-measured scattering cross section. An example of the output is given in Figs. 17 through 21.

The Westford program operation was described briefly in Sec. III. This program takes the reported analog-to-digital converter values, looks up the corresponding received power value in the calibration table, and calculates 1-sec average values of the received power. It also decodes time, antenna pointing, and doppler frequency data stored on the site tape, and calculates 1-sec averages of each of the quantities. Then, the program organizes the averaged data into tables for each scan. The determination of scan limits is either automatically made by the computer program or forced by card inputs. The data tables are recorded on magnetic tape; data are also plotted and printed for later editing and analysis.

The SDS 9300 computer at the Millstone Hill radar calculates most of the averages required for use of the radar data. The radar program takes the reported received power range square product and computes a backscatter cross section per unit volume for each range cell. From Eq. (6),

$$\beta_B = \left(\frac{1}{C_R P_t D}\right) P_r r_1^2$$

where C_R, P_t, and D are known constants for the radar determined from the values listed in Table III and discussed in Sec. IV. For ease in comparing the radar measurements with those obtained by other workers, the backscatter cross section per unit volume is reported as either an equivalent Z_e value or an equivalent C_{ne}^2 value [see Eqs. (7) and (10)]:

$$Z_e = \left(\frac{\lambda^2 \cdot 10^{17}}{\pi^5 |\kappa|^2 C_R T_t D}\right) P_r r_1^2 \tag{13}$$

$$C_{ne}^2 = \left(\frac{\lambda^{1/3} \cdot 10^7}{1.76\ C_R P_t D}\right) P_r r_1^2 \tag{14}$$

where the quantities in parentheses are constants for the radar, and the units are λ in centimeters, D in kilometers, P_r and P_t in the same units, r_1 in kilometers, C_R in cm^2, Z_e in mm^6/m^3 and C_{ne}^2 in $m^{-2/3}$.

The radar program calculates the transmission loss for comparison with the measured values using Eqs. (8), (9), (11), and (12)

$$\frac{1}{L} = A_R \sum_i G_2(\hat{\rho}_i)\, M_i Z_{ei} \frac{d}{\rho_i^2} \tag{15}$$

$$\frac{1}{L} = A_T \sum_i G_2(\hat{\rho}_i)\, M_i C_{nei}^2 \frac{d}{\rho_i^2} \left(\sin\frac{\varphi_i}{2}\right)^{-11/3} \tag{16}$$

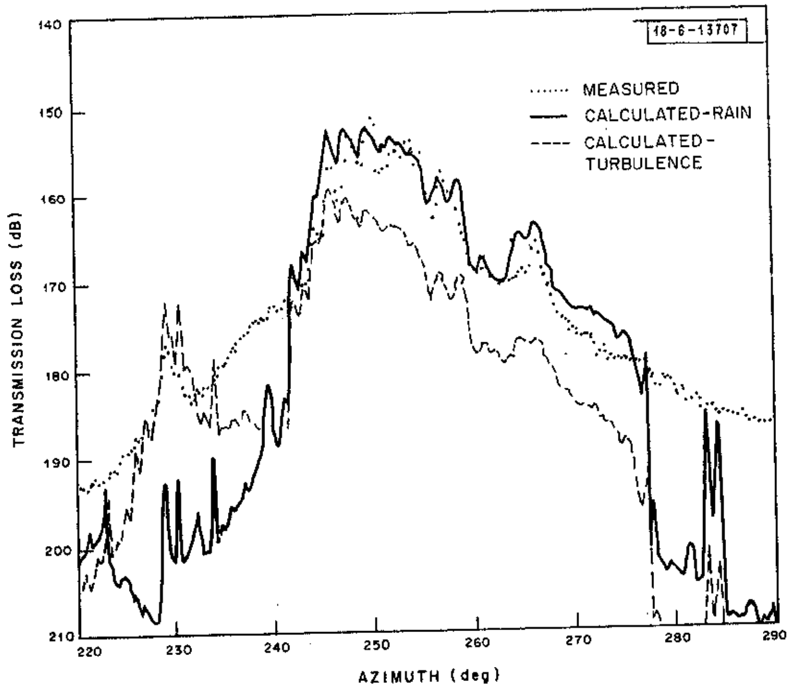

Fig. 19. Measured and calculated transmission losses. Westford: 1.5° elevation angle. Avon: 6° elevation angle; 23° azimuth; horn antenna.

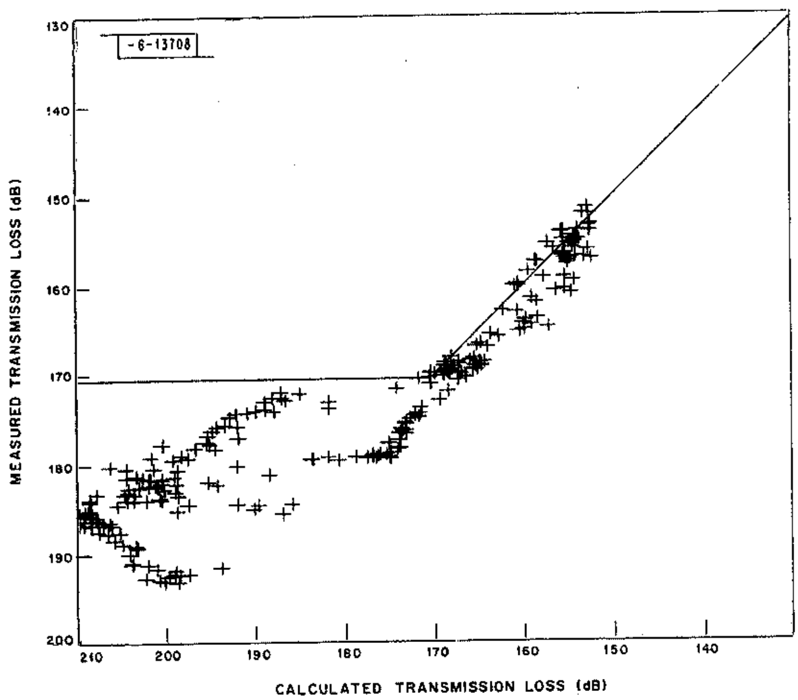

Fig. 20. Measured and calculated transmission losses due to rain. Westford: 1.5° elevation angle. Avon: 6° elevation angle; 23° azimuth; horn antenna.

I-6-13709

COMPARISON OF ESTIMATED AND MEASURED TRANSMISSION LOSS

	DIFFERENCES																	
	<-16	-16	-14	-12	-10	-8	-6	-4	-2	0	2	4	6	8	10	12	14	>14
-130	0	0	0	0	0	0	0	0	0	0	0	0	0	0	0	0	0	0
-132	0	0	0	0	0	0	0	0	0	0	0	0	0	0	0	0	0	0
-134	0	0	0	0	0	0	0	0	0	0	0	0	0	0	0	0	0	0
-136	0	0	0	0	0	0	0	0	0	0	0	0	0	0	0	0	0	0
-138	0	0	0	0	0	0	0	0	0	0	0	0	0	0	0	0	0	0
-140	0	0	0	0	0	0	0	0	0	0	0	0	0	0	0	0	0	0
-142	0	0	0	0	0	0	0	0	0	0	0	0	0	0	0	0	0	0
-144	0	0	0	0	0	0	0	0	0	0	0	0	0	0	0	0	0	0
-146	0	0	0	0	0	0	0	0	0	0	0	0	0	0	0	0	0	0
-148	0	0	0	0	0	0	0	0	0	0	0	0	0	0	0	0	0	0
-150	0	0	0	0	0	0	0	0	0	0	0	0	0	0	0	0	0	0
-152	0	0	0	0	0	0	0	0	1	2	0	0	0	0	0	0	0	0
-154	0	0	0	0	0	0	0	0	3	5	3	0	0	0	0	0	0	0
-156	0	0	0	0	0	0	0	0	1	3	6	1	0	0	0	0	0	0
-158	0	0	0	0	0	0	0	0	1	2	3	1	1	0	0	0	0	0
-160	0	0	0	0	0	0	0	0	1	3	1	3	2	0	0	0	0	0
-162	0	0	0	0	0	0	0	0	0	1	1	1	0	0	0	0	0	0
-164	0	0	0	0	0	0	0	0	0	0	0	4	2	0	0	0	0	0
-166	0	0	0	0	0	0	0	0	0	1	3	1	2	0	0	0	0	0
-168	0	0	0	0	0	0	0	0	0	4	2	2	0	0	0	0	0	0
-170	0	0	0	0	0	0	0	0	1	4	11	6	1	0	0	0	0	0
-172	0	3	2	0	0	0	0	0	1	0	2	1	0	0	0	0	0	0
-174	2	2	3	0	0	2	0	0	0	0	5	0	0	0	0	0	0	0
-176	4	2	0	0	0	0	0	0	0	0	8	0	0	0	0	0	0	0
-178	4	1	0	0	0	0	0	0	0	0	4	4	0	0	0	0	0	0
-180	8	0	0	1	0	0	0	2	1	1	2	4	2	0	0	0	0	0
-182	16	1	1	1	0	0	1	0	0	0	0	0	0	0	0	0	0	0
-184	10	2	3	0	0	1	1	0	1	0	0	0	0	0	0	0	0	0
-186	20	0	0	1	0	0	0	1	0	1	0	0	0	0	0	0	0	0
-188	4	1	0	0	0	0	0	0	0	0	0	0	0	0	0	0	0	0
-190	0	0	4	0	0	0	0	0	0	0	0	0	0	0	0	0	0	0
-192	0	0	0	2	2	4	3	0	1	0	0	0	0	0	0	0	0	0
-194	0	0	0	0	0	0	1	1	0	0	0	0	0	0	0	0	0	0
-196	0	0	0	0	0	0	0	0	0	0	0	0	0	0	0	0	0	0
-198	0	0	0	0	0	0	0	0	0	0	0	0	0	0	0	0	0	0
-200	0	0	0	0	0	0	0	0	0	0	0	0	0	0	0	0	0	0
-202	0	0	0	0	0	0	0	0	0	0	0	0	0	0	0	0	0	0
-204	0	0	0	0	0	0	0	0	0	0	0	0	0	0	0	0	0	0
-206	0	0	0	0	0	0	0	0	0	0	0	0	0	0	0	0	0	0
-208	0	0	0	0	0	0	0	0	0	0	0	0	0	0	0	0	0	0
-210	0	0	0	0	0	0	0	0	0	0	0	0	0	0	0	0	0	0
TOTAL	68	12	13	5	2	7	6	4	12	27	51	28	10	0	0	0	0	0

17-dB THRESHOLD

Fig. 21. Computer printout of comparison of measured and calculated transmission losses.

where

ρ_i = distance from transmitter (antenna 2) to the i^{th} range cell

d = range cell width

Z_{ei}, C_{nei}^2 = backscatter cross sections for the i^{th} range cell reported as Z_e or C_{ne}^2

$M_i = \hat{u}_1 \cdot (\hat{a}_1 \cos^2 \varphi_i \hat{a}_2 + \hat{b}_1 \hat{b}_2) \cdot \hat{u}_2$ evaluated for the i^{th} cell

φ_i = scattering angle for the i^{th} cell

$\sum_i$ = summation over range boxes

A_R, A_T = values given by Eqs. (9) and (12) using the parameters of the Westford Antenna listed in Table I and Sec. III.

The quantities M_i, φ_i, and ρ_i depend upon the location of the i^{th} cell with respect to the transmitter and the pointing angles of the transmit antenna. The transmitter location and transmit antenna pointing angles are entered by card input. Location of the i^{th} cell relative to the transmitter is computed using spherical geometry and, when refraction effects are important as in determining the height of the i^{th} cell above mean sea level, a 1.2 earth radius equivalent spherical earth is used. Figure 22 shows the relevant geometry and identifies the pointing and polarization vectors used in the computation. The local vertical at each location is specified by an unmarked arrow normal to lines of equal longitude. The pointing direction of the Millstone Hill antenna is given by $\hat{r}_1$, and the direction of propagation of the received signal by $\hat{k}_r = -\hat{r}_1$. The pointing direction of the Avon antenna is given by $\hat{\xi}$, and the direction of propagation from

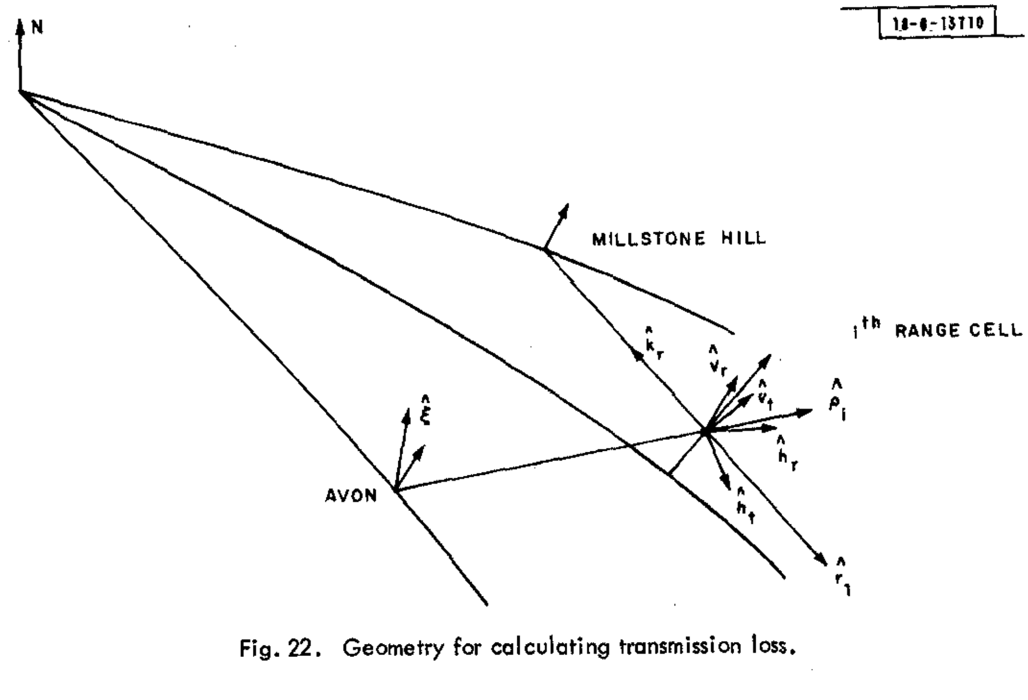

Fig. 22. Geometry for calculating transmission loss.

the antenna to the i^{th} cell by $\hat{\rho}_i$. Polarization vectors $\hat{v}_t$, $\hat{h}_t$ represent at the i^{th} cell the direction of the electric field vectors for vertical and horizontal polarization, respectively. Vectors $\hat{v}_r$, $\hat{h}_r$ give the polarization vectors for the Westford Antenna. The computer program calculates the three components of each of these vectors in a Cartesian coordinate system with $\hat{x}$ directed along the constant longitude line toward the south and $\hat{z}$ the local vertical. Given the vectors,

$$\varphi_i = \cos^{-1}(\hat{\rho}_i \cdot \hat{k}_r)$$

$$\hat{b}_1 = \hat{b}_2 = \frac{\hat{\rho}_i \times \hat{k}_r}{|\hat{\rho}_i \times \hat{k}_r|}$$

$$\hat{a}_2 = \frac{\hat{\rho}_i \times \hat{b}_2}{|\hat{\rho}_i \times \hat{b}_2|}$$

$$\hat{a}_1 = \frac{\hat{k}_r \times \hat{b}_1}{|\hat{k}_r \times \hat{b}_1|}$$

$$\hat{u}_1 = \hat{v}_r$$

$$\hat{u}_2 = \hat{v}_t \quad .$$

From these values, M_i is calculated. $G_2(\hat{\rho}_i)$ is found by expressing $\hat{\rho}_i$ in an angular coordinate system reference $\hat{\xi}$ and looking up the gain in a table. The tables reproduce the gain values given in Figs. 4 and 5.

Transmission loss is calculated for each pointing angle in the scan. For each transmission loss value, an expected rms error is also calculated based upon the uncertainty in the radar measurement and in the gain of the transmit antenna pattern. The antenna gain rms uncertainty is estimated by computing the transmission loss given by a hypothetical isotropic transmit antenna with a gain value 30 dB below the peak gain of the transmit antenna, and using the magnitude of ten times the logarithm of the value divided by the actual transmission loss value as the rms error. A computer output for a scan is shown in Fig. 17. Transmission loss was computed using Z_e and represents the expected loss for rain based upon the radar data. The set of three plotted lines gives the results of the calculation, with the upper and lower lines giving the calculated value plus and minus the expected rms error. Three other sets of calculated points are also plotted that give the results of computations using different combinations of transmit and receive antenna polarization. The computations were made by using either $\hat{h}$ or $\hat{v}$ for $\hat{u}$ in the calculation of M_i, as indicated on the plot legend. For comparison with the Westford measurements, the Millstone Hill azimuth values were parallax corrected to agree with those for Westford. The parallax correction was computed using the distance to the range cell that gives the maximum contribution to the value of transmission loss. The plotted azimuth values are for the Westford Antenna.

Transmission loss values measured on the Avon-to-Westford path were calculated by dividing the measured transmitter power value by the values of received power. Two representations of the measured data are plotted: the plotting with small dots gives the 1-sec average of the transmission loss, and that with the star gives the transmission loss value averaged over a beamwidth of the Millstone Hill radar centered about each parallax corrected azimuth value for the Millstone radar. The second set of values represents an approximate 6-sec average of the Westford measurements and agrees in pointing direction with the transmission loss calculations based upon the radar measurements. The additional factor of six in the averaging time also reduces the fluctuations inherent in the bistatic measurements.

The results of computations based upon turbulent layer scatter are given in Fig. 18. Figure 19 presents the rain and thin layer scatter computations for vertical polarization and the 6-sec averages of the measured transmission loss. These data were extracted from Figs. 17 and 18; they were also used in generating both the scattergram and the comparison table given in Figs. 20 and 21, respectively. The measured data agree well with the calculations based upon thin turbulent layer scatter in a region 6° wide about the great circle path (229.5° azimuth), and agree well with calculations based upon rain scatter in the 240° to 280° azimuth sector.

The scattergram (Fig. 20) presents the comparison between the measured and calculated transmission loss values for calculations based upon rain scatter. The length of the arms of each plotted cross represents the rms error in either the measurement or the calculation. For transmission loss values below 171 dB, agreement is evident; for measured values greater than 171 dB, poorer agreement is found. In this region, coupling via the Westford Antenna side lobes is important. However, this coupling has been ignored in the derivation of the equations used either to predict transmission loss or in the data processing. To approximately estimate the effect of side-lobe coupling, the transmission loss for a hypothetical isotropic receiving antenna with a gain 40 dB below that of the Westford Antenna was calculated. The transmission loss values were averaged over the entire scan to give an estimate of the threshold value for side-lobe effects. This value was used to position the horizontal line in Fig. 20. The value of 40 dB below the peak gain of the Westford Antenna was used to approximate the gain of the side lobes of the antenna out to a polar angle of 25° (see Fig. 7).

The comparison table for the ratio of calculated-to-measured cross section vs measured transmission loss is presented as a computer printout in Fig. 21. Data used to generate the scattergram were quantized in 2-dB intervals and used to generate the table. The column <-16 represents all occurrences of the measured signal being more than 17 dB or greater than the calculated value. This condition was used as a criterion to separate receiver side-lobe contributions from receiver main-lobe contributions. In Fig. 17, the comparison threshold value is shown as a horizontal line. All the measured data above this line were compared with the calculated values; measured data below the line were not used. It is noted that the values of transmission loss due to turbulent layer scatter are below the threshold and are ignored. The final comparison histogram is shown in Fig. 23 where the darkened bars represent the data above the side-lobe contamination threshold. These data were used to calculate the average and rms ratios of calculated-to-measured received signal strength or calculated-to-measured bistatic scatter cross sections. The measurement errors of both the radar system and the bistatic scatter system are multiplicative, the average and rms errors are all given in decibels in Tables II and IV. For this reason, the comparison is based upon the average and rms values of the logarithms of the ratio of the calculated-to-measured values. The average ratio is 0.6 dB and the rms ratio is 4.4 dB. Using linear averaging, the ratio is 2.1 dB. The linear average is biased toward overestimation and, if the ratio of measured-to-calculated cross section were used, a different ratio biased toward underestimation would be computed. Since the result for logarithmic averaging does not change

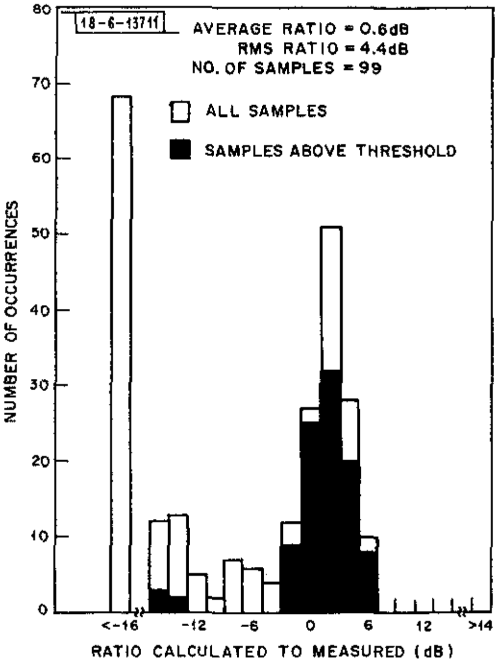

Fig. 23. Histogram of the ratio of calculated-to-measured scattering cross section. Westford: 1.5° elevation angle. Avon: 6° elevation angle; 23° azimuth; horn antenna.

with the way the ratio is made and since the errors are multiplicative, this form of averaging is used throughout for the analysis of the ratio of calculated-to-measured cross sections.

VI. SUMMARY

The measurement systems and the data processing programs were described in Secs. III through V. Results of the experiment are the statistics of the ratios of calculated-to-measured cross section as shown for one scan in Fig. 23. The measurement errors for the bistatic scatter system and for the radar system are tabulated in Tables II and IV. Errors in the estimate of the ratio of calculated-to-measured scattering cross section are given by the sum of the errors in Tables II and IV in the case of maximum error values, and of the square root of the sums of the squares for the rms errors. The combination procedure for the rms errors is adopted due to the multiplicative nature of the errors. Table V lists the errors in the estimate of the ratio. Three cases are considered: errors in the measurement of a single cell (a peak in received signal or minimum of transmission loss in a scan plot), errors in a scan or set of scans (one calibration), and errors for the entire measurement period (several calibrations). In computing the errors, the maximum error is assumed to be three times the rms error. The errors quoted in Table V apply when the correlation time for the bistatic scatter signal is the order of 200 msec with a 6-sec average. If the correlation time is still longer, the rms error will increase; if the correlation is shorter, the rms error will decrease. The rms error for the scan and all data averages will, however, not decrease significantly. For correlation times small in comparison with 20 msec, the average ratio of calculated-to-measured transmission loss should be decreased by 1.14 dB due to the integrating effect of the post-detection filter in the Westford receiver. The histogram given in Fig. 23 shows agreement between the measured and calculated cross sections because the average and rms ratios are within the error bounds. This is true independent of the correlation time because a 1.1-dB correction to the data for a correlation time small in comparison with 20 msec would produce an average ratio of −0.5 dB that is still well within the error bounds.

TABLE V ESTIMATION ACCURACY FOR THE RATIO OF CALCULATED-TO-MEASURED SCATTERING CROSS SECTION		
Data Base	Absolute Error Maximum (dB)	Fluctuation RMS (dB)
Single cell		
Horn, main lobe	4.6	1.2
Horn, far side lobe	13	1.2
4-foot, main lobe	4.8	1.2
4-foot, far side lobe	13	1.2
Single scan		
Horn	3.7	3.2
4-foot	3.9	3.2
All data		
Horn	2.7	3.2
4-foot	2.9	3.2

In summary, the Avon-to-Westford experiment is capable of comparing the measured and calculated bistatic scattering cross section of rain and thin turbulent layers with a maximum error in the ratio of the calculated-to-measured cross section of 2.7 dB and a probable error of much less. This test of the approximate description of rain and turbulent scatter is more precise than the allowable error in estimation of transmission loss due to these mechanisms; hence, the experiment provides a direct test of the approximations used in interference prediction techniques.

ACKNOWLEDGMENT

The author wishes to acknowledge the help and support of the staff of the Millstone Hill radar site and the staff of the Westford Communications site. Messrs. B.E. Nichols and H.H. Hoover of the latter site contributed much to the program. The effort of Mrs. Louise M. Balboni, who was responsible for the data processing programs, is also gratefully acknowledged.

The Westford and Millstone Hill facilities are supported by the Department of the Air Force under Contract F19628-70-C-0230.

REFERENCES

1. CCIR Report 339-1, "Influence of Scattering from Precipitation on the Siting of Earth Stations," XII Plenary Assembly, Vol. II, Part I, Propagation in Non-Ionized Media (International Telecommunications Union, Geneva, 1970).
2. R.K. Crane, "A Comparison Between Monostatic and Bistatic Scattering from Rain and Thin Turbulent Layers," Technical Note 1970-29, Lincoln Laboratory, M.I.T. (6 October 1970), DDC AD-N71-12395.
3. P.L. Rice, A.G. Longley, K.A. Norton and A.P. Barsis, "Transmission Loss Predictions for Tropospheric Communication Circuits," Vols. I and II, NBS Technical Note 101, U.S. Department of Commerce, Washington, D.C. (May 1965).
4. CCIR Report 244-2, "Estimation of Tropospheric-Wave Transmission Loss," XII Plenary Assembly, Vol. II, Part I, Propagation in Non-Ionized Media (International Telecommunications Union, Geneva, 1970).
5. R.K. Crane, "Microwave Scattering Parameters for New England Rain," Technical Report 426, Lincoln Laboratory, M.I.T. (3 October 1966), DDC AD-647798.
6. E.H. Grant, T.J. Buchanan and H.F. Cook, "Dielectric Behavior of Water at Microwave Frequencies," J. Chem. Phys. 26, 156 (1957).
7. V.I. Tatarski, Wave Propagation in a Turbulent Medium (McGraw-Hill, New York, 1961).
8. A. Cohen and A.W. Maltese, "The Lincoln Laboratory Antenna Test Range," Microwave J. 4, 57 (1961).
9. B.F. LaPage, E.W. Blaisdell and L.J. Ricardi, "West Ford Antenna and Feed System," Proc. IEEE 52, 589 (1964).
10. E.M.T. Jones, "Paraboloid Reflector and Hyperbolic Lens Antennas," Trans. IRE AP-2, 119 (1954).
11. M. Schwartz, W.R. Bennett and S. Stein, Communication Systems and Techniques, Inter-University Electronics Series Vol. 4 (McGraw-Hill, New York, 1966).
12. J.S. Marshall and W. Hitschfeld, "Interpretation of the Fluctuating Echo from Randomly Distributed Scatterers, Part I," Can. J. Phys. 31, 962 (1953).